

# **Landlab to FEniCSx : Finite Element Modeling of Shallow Water Equations**

9th May, 2025

## **MA5990: Project Report**

Under the guidance of

**Dr. Vettrivel V**

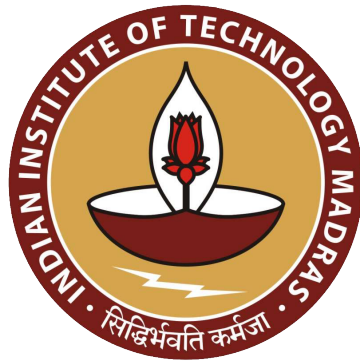
**Dr. Phil Weir**

**Ms. Kanika Miglani**

Submitted by

**Partha Sakha Paul**

**MA23M016**



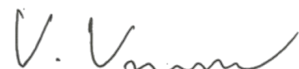
**Department of Mathematics  
Indian Institute of Technology Madras**

# THESIS CERTIFICATE

This is to certify that the thesis titled **Landlab to FEniCSx : Finite Element Modeling of Shallow Water Equations** submitted by **Partha Sakha Paul** to the Indian Institute of Technology Madras, for the **Mtech Project Thesis** is a bona fide record of the research work done by him under our supervision. The contents of this thesis, in full or in parts, have not been submitted to any other Institute or University for the award of any degree or diploma.

## Research Guides

Chennai, India



डॉ. वि. वेट्रिवेल/Dr. V. VETRIVEL  
प्राच्यापक्ष/PROFESSOR  
मैथेमेटिक्स विभाग  
भारतीय प्रौद्योगिकी संस्थान चेन्ऩई<sup>१००००३६</sup>  
DEPARTMENT OF MATHEMATICS  
INDIAN INSTITUTE OF TECHNOLOGY MADRAS  
CHENNAI / CHENNAI - 600 036

**Dr. Vetrivel V**  
(Professor, Department of Mathematics, IIT Madras)

Belfast, Northern Ireland

  
**Dr. Phil Weir**  
(Director, Flax & Teal Ltd.)

Bangalore, India

  
**Ms. Kanika Miglani**  
(Data Scientist, Flax & Teal Ltd.)

## ACKNOWLEDGEMENTS

I am deeply grateful to my guide, **Dr. Vetrivel V**, from the Department of Mathematics, IIT Madras, for his invaluable guidance, strong support, and constant encouragement throughout this project. His expertise and insightful advice have played a crucial role in shaping my understanding and approach to this research, and I sincerely appreciate his patience and dedication.

I sincerely thank Flax and Teal Ltd. for giving me the opportunity to work on such a valuable and complex real-world problem. I am truly grateful to **Dr. Phil Weir**, Director of Flax and Teal Ltd. for his inspiring leadership, regular guidance and support throughout my internship. I express my grateful appreciation to **Dr. Jørgen S. Dokken**, Senior Research Engineer at Simula Research Laboratory for his invaluable help in deepening my understanding of the FEniCSx library, and to **Dr. Ellery Ames**, Scientific Software Engineer at Flax and Teal Ltd. for their insightful guidance on the finite element method for Shallow Water Equations. I extend my heartfelt appreciation to **Ms. Kanika Miglani**, Data Scientist at Flax and Teal Ltd., for being the Co-guide and managing my project, her careful coordination, thoughtful guidance, and continuous encouragement, which played a key role in the successful completion of this project.

I would like to thank the Department of Mathematics, IIT Madras, for providing the necessary facilities and a supportive environment to conduct my work on campus.

I would also like to express my gratitude to my colleagues at Flax and Teal Ltd. for their support throughout my project. I am truly grateful for the financial support from Flax and Teal Ltd. through the stipend during my internship. This support allowed me to concentrate fully on my work without any worries. I am truly grateful for their confidence in my abilities and for creating an environment that nurtured learning and innovation.

I sincerely appreciate the developers of the open-source libraries that were essential to this research, including NumPy, Matplotlib, rasterio, imageio, pandas, Docker Desktop, and DOLFINx. I also acknowledge the valuable contributions of the scientific community in advancing computational modeling and numerical methods.

Finally, I am deeply thankful to my family and friends for their constant support, patience, and encouragement throughout this journey. Their constant faith in me has been a continual source of strength and inspiration.

# ABSTRACT

**Keywords:** Finite Element Method (FEM), Finite Volume Method (FVM), Overland Flow, FEniCSx, Saint-Venant Equations (SWEs), Continuous Galerkin (CG), Discontinuous Galerkin (DG), Wetting-Drying Algorithm, Numerical Fluxes.

The OverlandFlow model in Landlab, a finite volume-based solver for overland flow dynamics, provides a robust framework for simulating shallow water equations (SWEs). However, finite element methods (FEM) offer potential advantages in flexibility and accuracy, particularly for complex topographies. This project focuses on developing a finite element-based SWE solver in FEniCSx, converting the OverlandFlow model from a finite volume (FVM) formulation to a FEM approach.

The numerical implementation employs the Saint-Venant equations, discretized using continuous Galerkin (CG) and discontinuous Galerkin (DG) formulations for 1D and 2D shallow water flows. A key aspect of this work involves handling boundary conditions weakly to ensure numerical stability and implementing numerical fluxes to reduce oscillations in high-gradient regions. Additionally, a wetting-drying algorithm inspired by the SWEMniCS paper has been integrated to track dynamic wet-dry interfaces accurately.

The model's performance is assessed by comparing FEM and FVM solutions across different Manning's coefficients, flow velocities, and mesh resolutions in 1D. For 2D simulations, both CG and DG formulations are explored. DG methods demonstrate superior numerical stability due to the incorporation of numerical fluxes, making them particularly effective in handling discontinuities.

This study demonstrates that FEM can effectively model shallow water flows with competitive accuracy compared to FVM. The findings contribute to the advancement of finite element-based hydrodynamic solvers using open-source frameworks like FEniCSx.

# TABLE OF CONTENTS

<b>ACKNOWLEDGEMENTS</b>	i
<b>ABSTRACT</b>	ii
<b>LIST OF FIGURES</b>	v
<b>LIST OF TABLES</b>	vi
<b>LIST OF NOTATIONS</b>	vii
<b>LIST OF ABBREVIATIONS</b>	viii
<b>1 INTRODUCTION</b>	1
1.1 Background . . . . .	1
1.2 Research Problem and Justification . . . . .	1
1.3 Objective . . . . .	1
1.4 Research Questions . . . . .	2
1.5 Scope and Limitations . . . . .	2
<b>2 LITERATURE REVIEW</b>	3
2.1 Summary of Previous Research . . . . .	3
2.2 Theoretical Framework . . . . .	3
2.3 Identification of Research Gaps & Justification . . . . .	3
2.4 Critical Analysis of Existing Work . . . . .	4
<b>3 METHODOLOGY</b>	5
3.1 SWEs in 1D : Mathematical Formulation of the Finite Element Model . . . . .	5
3.1.1 Assumptions . . . . .	6
3.1.2 Simplified System by the assumptions . . . . .	6
3.1.3 Finite Element Formulation . . . . .	7
3.1.4 Test 1: Nonbreaking Wave Propagation Over a Horizontal Plane . . . . .	7
3.1.5 Finite Element Method (FEM) Implementation . . . . .	8
3.2 SWEs in 2D : Mathematical Formulation of the Finite Element Model . . . . .	8
3.2.1 2D model proposed by <i>Bates et al.</i> . . . . .	8
3.2.2 2D model: Full Conservation Form . . . . .	10
<b>4 RESULTS AND DISCUSSION</b>	15
4.1 SWEs in 1D: Test 1 (Comparison of FEM and FVM) . . . . .	15
4.1.1 Simulation Setup . . . . .	15
4.1.2 Mesh Resolution and Numerical Stability . . . . .	15
4.1.3 Effect of Time Step on Mesh Resolution in FEM . . . . .	17
4.2 SWEs in 2D: Results . . . . .	18
4.2.1 Test 2: SWEs 2D - Without Bathymetry Experiment with Tidal Wave . . . . .	18
4.2.2 Test Case Study 1: SWEs on a 2D Sloped Beach (Continuous Galerkin) . . . . .	20

4.2.3	Test Case Study 2: SWEs on a 2D Sloped Beach (Discontinuous Galerkin) . . . . .	23
4.2.4	Test 3: SWEs on Real DEM Bathymetry . . . . .	25
<b>5</b>	<b>CONCLUSION AND FUTURE WORK</b>	<b>27</b>
5.1	Summary of Key Findings . . . . .	27
5.2	Answering Research Questions . . . . .	27
5.3	Practical Applications . . . . .	28
5.4	Expectations for Future Research . . . . .	29
<b>APPENDIX</b>		<b>30</b>
A.1	Numerical Methods . . . . .	30
A.1.1	Finite Element Method for Advection . . . . .	30
A.1.2	Finite Volume Methods for SWE . . . . .	30
A.1.3	FEM for SWE in 2D . . . . .	30
A.2	Additional Figures . . . . .	30
A.2.1	Test 2: Bathymetry Description . . . . .	30
A.2.2	Test Case Study 1 & 2: Bathymetry Description . . . . .	31
A.2.3	Test 3: Bathymetry Description . . . . .	32
A.3	Processing the DEM Data . . . . .	33
<b>REFERENCES</b>		<b>34</b>

## LIST OF FIGURES

1	Comparison of FEM (top row) and FVM (bottom row) results for the 1D Shallow Water Equations . . . . .	16
2	Test 2 (without bathymetry) - Surface elevation and velocity components at station (9000, 3650) m. . . . .	18
3	Test 2 (without bathymetry) - Surface elevation and velocity components at station (11000, 3650) m. . . . .	19
4	Test 2 (without bathymetry) - Surface elevation and velocity components at station (13500, 3650) m. . . . .	19
5	Test Case Study 1 (Sloped Beach - CG): Water Surface Elevation and X-Velocity at Station 1 . . . . .	21
6	Test Case Study 1 (Sloped Beach - CG): Water Surface Elevation and X-Velocity at Station 2 . . . . .	22
7	Test Case Study 1 (Sloped Beach - CG): Water Surface Elevation and X-Velocity at Station 3 . . . . .	22
8	Test Case Study 2 (Sloped Beach - DG): Water Surface Elevation and X-Velocity at Station 1 . . . . .	23
9	Test Case Study 2 (Sloped Beach - DG): Water Surface Elevation and X-Velocity at Station 2 . . . . .	24
10	Test Case Study 2 (Sloped Beach - DG): Water Surface Elevation and X-Velocity at Station 3 . . . . .	24
11	Test 3 (with real bathymetry) - WSE at Different Stations . . . . .	25
12	Test 3 (with real bathymetry) - X-Velocity at Different Stations . . . . .	26
13	Test 2: Bathymetry . . . . .	30
14	Test Case Study 1 & 2: Bathymetry . . . . .	31
15	Test 3: Bathymetry . . . . .	32

## LIST OF TABLES

1	Simulation parameters for both test cases in 1D . . . . .	15
2	Summary of Experiments and Corresponding Figures . . . . .	16
3	$L_2$ Errors for Water Surface Elevation and Velocities at Different Stations (CG) . . . . .	20
4	$L_2$ Errors for Water Surface Elevation and Velocities at Different Stations (DG) . . . . .	23

# LIST OF NOTATIONS

## ⌚ Mathematical Symbols:

Symbol	Description	Unit
$h$	Water depth	$m$
$z$	Elevation of the bathymetry	$m$
$H$	Total water depth including bathymetry	$m$
$q_x, q_y$	Discharge components in $x$ and $y$ directions	$m^2/s$
$u_x, u_y$	Velocity components in $x$ and $y$ directions	$m/s$
$g$	Gravitational acceleration	$m/s^2$
$n$	Manning's roughness coefficient	$s/m^{1/3}$
$\Delta x, \Delta t$	Spatial and temporal step sizes	$m, s$
$h^{(n+1)}$	Value of $h$ at the next time step	$m$
$h^{(n)}$	Value of $h$ at the current time step	$m$
$h^{(n-1)}$	Value of $h$ at the previous time step	$m$
$T$	Total simulation time	$s$
$\Omega$	Computational domain	
$\partial\Omega$	Boundary of computational domain	
$\Gamma$	Boundary of the domain	
$\Gamma_w$	Wall boundary of the domain (ds(1))	
$\Gamma_o$	Open boundary of the domain (ds(2))	

## ⌚ Finite Element Terms:

$V_h$	Finite element function space
$v^{(\text{in})}$	Value of $v$ at the interior of an element of the domain
$v^{(\text{out})}$	Value of $v$ at the exterior of an element of the domain
$\mathbf{n}$	Unit outward normal to the boundary

## ⌚ Numerical Parameters:

$\theta$	Time-stepping parameter (e.g., for implicit methods)
$nx, ny$	Number of elements in the x and y directions in the domain respectively

## LIST OF ABBREVIATIONS

PDE	Partial Differential Equation
SWE	Shallow Water Equation
FE	Finite Element
FEM	Finite Element Method
FEniCSx	An open-source platform helps to solve PDEs using FEM
FVM	Finite Volume Method
WSE	Water Surface Elevation
CG	Continuous Galerkin
DG	Discontinuous Galerkin
SUPG	Streamline Upwind Petrov-Galerkin
CFL	Courant–Friedrichs–Lewy
DEM	Digital Elevation Model
ML	Machine Learning
AI	Artificial Intelligence

# 1 INTRODUCTION

## 1.1 Background

Shallow water equations (SWEs) are widely used in hydrodynamic modeling to simulate *overland flow, river hydraulics, coastal dynamics, and flood propagation*. Traditional numerical methods for solving SWEs include **FVM** and **FEM**. The **OverlandFlow model**<sup>16</sup> in **Landlab**, based on FVM, is a widely used approach for overland flow modeling. However, FEM provides greater flexibility with **complex geometries, adaptive meshing, and higher-order approximations**, making it an attractive alternative.

While **FVM**<sup>1</sup> ensures mass conservation and sharp shock capturing<sup>17</sup>, FEM provides advantages in terms of **numerical stability and smooth solutions** for problems with continuous topography and variable terrain conditions. The development of open-source finite element libraries such as **FEniCSx**<sup>7</sup> has made it suitable to implement and explore FEM-based solutions for SWE problems.

This study focuses on developing a **finite element-based SWE solver** in **FEniCSx**, translating the OverlandFlow model from **FVM to FEM**. Additionally, **CG and DG formulations** are explored to assess their impact on solution quality.

## 1.2 Research Problem and Justification

Although FVM works well for solving SWEs, it can be difficult to use with **complicated shapes and changing mesh sizes**. FEM, on the other hand, provides an efficient framework for solving differential equations on irregular domains but is less commonly used for overland flow modeling. A key challenge in FEM-based SWE solvers is **ensuring numerical stability**<sup>18</sup>, particularly in handling **boundary conditions, numerical fluxes**.

Preliminary experiments showed that FEM solutions can **oscillate at coarse resolutions (20–70 elements)** but become more stable at **finer resolutions (above 90 elements)**, matching FVM results in 1D. Additionally, **reducing the time step allows FEM to produce accurate results even with fewer elements**, highlighting an important **trade-off between spatial and temporal resolution**.

The findings of this study are expected to **contribute to the development of FEM-based hydrodynamic solvers** that can be used in flood modeling applications.

## 1.3 Objective

The main objective of this study is to **develop and validate a finite element-based SWE solver in FEniCSx** by comparing its performance with finite volume methods. The specific objectives are:

- Implement and convert FVM-based formulations into FEM framework for solving the SWEs in 1D & 2D.
- Analyze numerical accuracy and stability by comparing FEM solutions (CG and DG) with FVM results.

- Investigate the wetting-drying algorithm inspired by the *SWEMniCS* paper.

## 1.4 Research Questions

The development of open-source finite element libraries such as **FEniCSx** has made it possible to implement and explore FEM-based solutions for shallow water equations (SWEs).

Finite element methods offer flexibility in handling complex geometries and boundary conditions, but their accuracy is highly dependent on mesh resolution and time step size. This leads to a inquiry: **Investigation of the trade-off between the effect of mesh resolution and time step size on the quality of FEM solutions.**

Numerical stability remains a challenge in FEM-based SWE solvers, especially when dealing with high-gradient flows or discontinuities or in dry area. Another aspect of SWE modeling is **how numerical flux stabilization techniques can improve solution accuracy.**

Another aspect of SWE modeling is the wetting and drying processes, which are essential for accurately capturing real-world hydrodynamics. An important consideration is **the effectiveness of the wetting-drying algorithm in capturing dynamic water surface transitions.**

Addressing these research questions will contribute to a deeper understanding of FEM's capabilities for solving SWEs and help to fill the gap between FEM and traditional finite volume methods in hydrodynamic modeling.

## 1.5 Scope and Limitations

This study focuses on solving the **1D and 2D SWEs using FEM** in FEniCSx, comparing the results with **FVM-based OverlandFlow solutions in 1D**. The study is limited to:

- **Idealized test cases** with controlled initial and boundary conditions.
- **Structured meshes**, future extensions may include adaptive meshing techniques.
- **Comparisons with FVM from the SWE Paper**, rather than implementing a fully coupled multi-physics model.

While the project explores **CG and DG formulations**, the emphasis is on numerical stability, boundary condition handling, and wetting-drying techniques, rather than **high-order FEM methods**.<sup>1</sup>

---

<sup>1</sup>All test cases and case studies, along with detailed instructions for execution, are available in the Git repository: [FEniCS\\_Landlab](#)

## 2 LITERATURE REVIEW

### 2.1 Summary of Previous Research

Traditional numerical approaches utilize the **FVM** due to its robustness in handling shock waves and ensuring mass conservation. *Almeida et al.*<sup>1</sup> introduced modifications to enhance the numerical stability of simple SWEs formulations for two-dimensional flood modeling, emphasizing the importance of stability in FVM applications.

The FEM has gained attraction for solving SWEs, particularly through Continuous Galerkin (CG) and Discontinuous Galerkin (DG) formulations. The rise of open-source finite element libraries, **SWEMniCS**<sup>2</sup>, offers a comprehensive toolbox for modeling coastal ocean circulation, storm surges, and compound flooding, integrating advanced numerical stabilization techniques and wetting-drying algorithms to enhance simulation accuracy.<sup>2</sup>

### 2.2 Theoretical Framework

The numerical solution of SWEs depends on discretization methods that balance accuracy, stability, and computational efficiency. FVM approaches discretize the domain into **control volumes**, applying integral conservation laws to ensure robustness, especially in capturing shocks and discontinuities. However, FVM may face challenges in achieving higher-order accuracy.

FEM utilizes **basis functions** to approximate solutions, offering flexibility in handling complex geometries and facilitating higher-order accuracy. The **DG variant of FEM**, in particular, has been known for its local conservation properties and suitability for problems dominated by advection.

Stabilization techniques are crucial in numerical simulations to reduce oscillations and enhance solution stability. SWEMniCS incorporates **flux-based stabilization** methods, which are the basis for improving the stability of FEM-based SWE solvers. In addition, accurately modeling **wetting-drying**<sup>6</sup> processes is crucial for realistic simulations. SWEMniCS addresses this by implementing sophisticated algorithms that ensure smooth transitions between wet and dry states, thereby preserving the physical integrity of the model<sup>2</sup>.

### 2.3 Identification of Research Gaps & Justification

Despite significant advancements, several areas require further investigation:

- **Comparative Analyses:** There are few studies<sup>12</sup> that systematically compare the accuracy, stability, and computational efficiency of finite element and finite volume methods for solving shallow water equations across different scenarios. Developed and evaluated CG and DG FEM formulations against FVM solutions for SWEs.

---

<sup>2</sup>For a detailed discussion on numerical methods, including Advection PDE, FEM and FVM for SWEs, see Appendix A.1.

- **Stabilization Techniques in FEM:** Although flux-based stabilization methods exist, their effectiveness in different FEM formulations (CG vs. DG) is not well studied.
- **Mesh and Time Step Sensitivity:** The trade-off between mesh resolution, time step size, and solution quality in FEM-based approaches requires a deeper understanding to inform optimal meshing and time-stepping strategies.  
Explored how variations in mesh resolution and time step size influence the accuracy and stability of FEM solutions, providing optimal discretization practices for 1D.
- **Wetting-Drying Algorithm Validation:** Existing wetting-drying algorithms, though advanced, require detailed validation against empirical data to ensure their accuracy and reliability in diverse modeling scenarios.  
The validation of wetting-drying methods implemented in FEM for SWEs in 2D has been conducted with real-world data to ensure model reliability.

By examining these aspects, this study seeks to validate the stability of numerical simulations for SWEs, providing useful insights for both research and real-world hydrodynamic modeling.

## 2.4 Critical Analysis of Existing Work

The literature reflects a perfect foundation in numerical methods for SWEs, with both FVM and FEM demonstrating distinct advantages. Almeida et al.<sup>1</sup> focused on **enhancing FVM stability**, presenting modifications that significantly improved model performance in flood simulations. Conversely, *Clint Dawson*<sup>2</sup> demonstrated the effectiveness of **DG-FEM** for solving the shallow water equations, highlighting its ability to handle complex coastal and flood dynamics with **numerical flux stabilization and wetting-drying techniques**.

SWEMniCS stands out as a key tool; however, the need for direct comparative studies between FEM and FVM, as well as **empirical validation of numerical methods**, remains evident.

### 3 METHODOLOGY

#### 3.1 SWEs in 1D : Mathematical Formulation of the Finite Element Model

For deriving the mathematical formulation used in the model is the full-dynamic version of the one-dimensional Saint-Venant equations<sup>1</sup>. These equations describe the conservation of mass and momentum in open channel flow:

The continuity equation is given by:

$$\frac{\partial A}{\partial t} + \frac{\partial Q}{\partial x} = 0, \quad (1)$$

This equation represents the principle of conservation of mass in one-dimensional open channel flow. It states that **the rate of change of the flow area with respect to time, combined with the spatial variation of discharge, must be zero** - ensuring that **mass is neither created nor lost within a control volume**.

The notations used in the continuity equation are as follows:

- $A$  [ $\text{m}^2$ ]: Cross-sectional area of flow, representing the area of the water column perpendicular to the flow direction.
- $Q$  [ $\text{m}^3 \cdot \text{s}^{-1}$ ]: Discharge or volumetric flow rate, which is the volume of water passing through a cross-section per unit time.
- $x$  [ $\text{m}$ ]: Longitudinal coordinate along the flow direction.
- $t$  [ $\text{s}$ ]: Time variable, representing temporal evolution of the flow.

The momentum equation is expressed as:

$$\underbrace{\frac{\partial Q}{\partial t}}_{\text{local acceleration}} + \underbrace{\frac{\partial}{\partial x} \left( \frac{Q^2}{A} \right)}_{\text{convective acceleration}} + \underbrace{gA \frac{\partial(h+z)}{\partial x}}_{\text{pressure and bed gradients}} + \underbrace{gn^2 \frac{|Q|Q}{R^{4/3}A}}_{\text{friction}} = 0, \quad (2)$$

Each term in this equation represents a distinct physical effect in open channel flow:

- $\frac{\partial Q}{\partial t}$  (**Local acceleration**): Accounts for the temporal change in discharge at a fixed location, representing unsteady flow effects.
- $\frac{\partial}{\partial x} \left( \frac{Q^2}{A} \right)$  (**Convective acceleration**): Describes the spatial variation of momentum due to changes in discharge, relevant in rapidly varying flows.
- $gA \frac{\partial(h+z)}{\partial x}$  (**Pressure and bed slope effects**): Captures the combined effect of hydrostatic pressure gradient and bed slope, which are the driving forces in SWEs.
- $gn^2 \frac{|Q|Q}{R^{4/3}A}$  (**Frictional resistance**): Represents energy loss due to friction, modeled using Manning's equation<sup>1</sup>. This nonlinear term depends on the discharge, hydraulic radius, and roughness coefficient.

The following notations are used in the momentum equation:

- $h$  [m]: Water depth measured from the mean sea level to the free surface.
- $z$  [m]: Bed elevation, representing the vertical position of the channel bottom.
- $R$  [m]: Hydraulic radius, defined as the cross-sectional area( $A$ ) divided by the wetted perimeter( $P$ )<sup>21</sup>. It characterizes the shape of the flow and affects frictional resistance.
- $n$  [ $s \cdot m^{-1/3}$ ]: Manning's roughness coefficient, an empirical parameter representing the resistance exerted by the bottom channel surface of the flow.

### 3.1.1 Assumptions

The derivation of the below system is based on the following assumptions<sup>1</sup>:

- **The convective acceleration term in the momentum equation is neglected.**  
This means changes in momentum due to velocity variations along the flow are considered insignificant compared to other forces such as gravity and friction.
- **The hydraulic radius  $R$  is approximated as the water depth  $h$ , implying negligible lateral friction effects (a shallow water property).**  
This simplification is valid in wide channels or overland flow where the width is much greater than the depth, so the influence of side boundaries on flow resistance becomes negligible.
- **The flow is assumed to be shallow, and the influence of vertical acceleration is ignored.**  
Vertical velocity components and pressure variations in the vertical direction are assumed hydrostatic, simplifying the 3D flow behavior to a 2D horizontal model.
- **The frictional resistance follows Manning's equation.<sup>2</sup>**  
This empirical formula relates flow resistance to bottom-bed roughness, used for open channel and overland flow modeling.

### 3.1.2 Simplified System by the assumptions

By neglecting the convective acceleration term in Equation (2), dividing by the width  $b$  (where  $A = bh$ ), and assuming  $R = h$  (i.e., neglecting lateral friction), the following simplified system is obtained:

$$\frac{\partial h}{\partial t} + \frac{\partial q}{\partial x} = 0, \quad (\text{Continuity Equation}) \quad (3)$$

$$\frac{\partial q}{\partial t} + gh \frac{\partial(h+z)}{\partial x} + gn^2 \frac{|q|q}{h^{7/3}} = 0. \quad (\text{Momentum Equation}) \quad (4)$$

where

- $b$  [m] width of the cross-section,
- $q (= \frac{Q}{b})$  [ $m^2 \cdot s^{-1}$ ] is the discharge per unit width

### 3.1.3 Finite Element Formulation

To convert these equations into a finite element framework, we seek weak form representations. Multiplying equation (3) by suitable test function and integrating over the domain yields the weak form necessary for implementation in a FEM solver.

The governing continuity equation for the shallow water equations (SWE) is given by:

$$\frac{\partial h}{\partial t} + \frac{\partial q}{\partial x} = 0, \quad (5)$$

where the discharge per unit width is defined as:

$$q = hu. \quad (6)$$

Replacing  $q$  and expanding the equation using the product rule and then multiplying by a test function  $v$  and integrating over the domain  $\Omega$ :

$$\int_{\Omega} \frac{h^{(n+1)} - h^{(n)}}{\Delta t} v \, dx + \int_{\Omega} h \frac{\partial u}{\partial x} v \, dx + \int_{\Omega} u \frac{\partial h}{\partial x} v \, dx = 0. \quad (7)$$

Rearranging:

$$\int_{\Omega} h^{(n+1)} v \, dx + \Delta t \int_{\Omega} h \frac{\partial u}{\partial x} v \, dx + \Delta t \int_{\Omega} u \frac{\partial h}{\partial x} v \, dx = \int_{\Omega} h^{(n)} v \, dx. \quad (8)$$

If  $u$  is constant, then  $\frac{\partial u}{\partial x} = 0$ , simplifying the weak form to:

$$\int_{\Omega} h^{(n+1)} v \, dx + \Delta t \int_{\Omega} u \frac{\partial h}{\partial x} v \, dx = \int_{\Omega} h^{(n)} v \, dx. \quad (9)$$

This final expression represents the weak form of the continuity equation in the finite element framework.

### 3.1.4 Test 1: Nonbreaking Wave Propagation Over a Horizontal Plane

The first numerical experiment examines the propagation of a wave over a horizontal plane (i.e.,  $\frac{\partial z}{\partial x} = 0$ ) where the initial condition corresponds to a dry state.

Under a specific set of boundary conditions, this problem has an exact solution to the full-dynamic shallow water equations, serving as a reliable benchmark for evaluating the model's precision.

*Hunter et al.* (2005) initially proposed this solution along with the associated boundary conditions, assuming a uniform velocity distribution in the direction of wave propagation. A concise overview of this solution is presented here.

The SWEs in 1D considered for this experiment are:

$$\frac{\partial h}{\partial t} + u \frac{\partial h}{\partial x} = 0. \quad (10)$$

$$\frac{\partial u}{\partial t} + u \frac{\partial u}{\partial x} + g \left( \frac{\partial h}{\partial x} + \frac{\partial z}{\partial x} \right) + g \frac{n^2 u^2}{h^{4/3}} = 0. \quad (11)$$

For this experiment, we assume that the velocity  $u$  is constant, simplifying the system. From equation (11), we obtain:

$$\frac{\partial h}{\partial x} = -\frac{\partial z}{\partial x} + \frac{n^2 u^2}{h^{4/3}}. \quad (12)$$

The depth  $h(x, t)$  evolves according to (10) by Lagrange Equations:

$$h(x, t) = h(x - ut, 0). \quad (13)$$

The solution for  $h$  is derived from equation (12):

$$h = \left[ -\frac{7}{3} (n^2 u^2 x + C) \right]^{3/7}. \quad (14)$$

Applying the moving boundary condition  $h(ut, t) = 0$  gives:

$$C = -n^2 u^2 (ut) \quad (15)$$

which results in the final solution:

$$h(x, t) = \left[ -\frac{7}{3} n^2 u^2 (x - ut) \right]^{3/7}. \quad (16)$$

At  $x = 0$ , we get:

$$h(0, t) = \left( \frac{7}{3} n^2 u^3 t \right)^{3/7}. \quad (17)$$

### 3.1.5 Finite Element Method (FEM) Implementation

In the weak formulation, we define the variational form as:

$$\int \left( \frac{h}{dt} v + u \frac{\partial h}{\partial x} v \right) dx = \int \frac{h_{\text{prev}}}{dt} v dx. \quad (18)$$

The boundary condition at  $x = 0$  follows equation (17):

$$h(0, t) = \left( \frac{7}{3} n^2 u^3 t \right)^{3/7}. \quad (19)$$

The finite element method implementation follows the same initial and boundary conditions as the finite volume method from the SWE paper. The FEM formulation successfully captures the evolution of  $h(x, t)$  under the given conditions and provides comparable results.

## 3.2 SWEs in 2D : Mathematical Formulation of the Finite Element Model

### 3.2.1 2D model proposed by *Bates et al.*

In the two-dimensional model introduced by *Bates et al.* (2010), a simplified form<sup>1</sup> of the one-dimensional momentum conservation equation (2) is employed to approximate the

flow exchange between adjacent cells. Meanwhile, the two-dimensional continuity equation is utilized to establish the coupling between the  $x$ - and  $y$ -directions. This formulation results in the following system of three partial differential equations:

$$\frac{\partial h}{\partial t} + \frac{\partial q_x}{\partial x} + \frac{\partial q_y}{\partial y} = 0, \quad (20)$$

$$\frac{\partial q_x}{\partial t} + gh \frac{\partial(h+z)}{\partial x} + gn^2 \frac{|q_x|q_x}{h^{7/3}} = 0, \quad (21)$$

$$\frac{\partial q_y}{\partial t} + gh \frac{\partial(h+z)}{\partial y} + gn^2 \frac{|q_y|q_y}{h^{7/3}} = 0. \quad (22)$$

where,

- $h$  is the free surface height.
- $(q_x, q_y)$  momentum components in the  $x$  and  $y$  directions.
- $g$  is the gravitational acceleration.
- $n$  is the Manning's roughness coefficient, which accounts for bottom friction.

**Weak Formulation** The governing equations for shallow water flow are expressed in the weak form as:

$$\int_{\Omega} \left( \frac{\partial h}{\partial t} v_h + \frac{\partial(hu_x)}{\partial x} v_h + \frac{\partial(hu_y)}{\partial y} v_h \right) d\Omega = 0, \quad (23)$$

$$\int_{\Omega} \left( \frac{\partial(hu_x)}{\partial t} v_{u_x} + gh \frac{\partial(h+z)}{\partial x} v_{u_x} + gn^2 \frac{|u_x|u_x}{h^{1/3}} v_{u_x} \right) d\Omega = 0, \quad (24)$$

$$\int_{\Omega} \left( \frac{\partial(hu_y)}{\partial t} v_{u_y} + gh \frac{\partial(h+z)}{\partial y} v_{u_y} + gn^2 \frac{|u_y|u_y}{h^{1/3}} v_{u_y} \right) d\Omega = 0. \quad (25)$$

Time discretization using the backward Euler scheme gives:

$$\int_{\Omega} \left( \frac{h - h_{\text{prev}}}{\Delta t} v_h + \frac{\partial(hu_x)}{\partial x} v_h + \frac{\partial(hu_y)}{\partial y} v_h \right) d\Omega = 0, \quad (26)$$

$$\int_{\Omega} \left( \frac{hu_x - (hu_x)_{\text{prev}}}{\Delta t} v_{u_x} + gh \frac{\partial(h+z)}{\partial x} v_{u_x} + gn^2 \frac{|u_x|u_x}{h^{1/3}} v_{u_x} \right) d\Omega = 0, \quad (27)$$

$$\int_{\Omega} \left( \frac{hu_y - (hu_y)_{\text{prev}}}{\Delta t} v_{u_y} + gh \frac{\partial(h+z)}{\partial y} v_{u_y} + gn^2 \frac{|u_y|u_y}{h^{1/3}} v_{u_y} \right) d\Omega = 0. \quad (28)$$

where,

- $v_h, v_{q_x}, v_{q_y}$ : Test functions in the finite element method.
- $(u_x, u_y)$ : Velocity components in the  $x$  and  $y$  directions.
- $\Omega$ : Computational domain.
- $h_{\text{prev}}, q_{x,\text{prev}}, q_{y,\text{prev}}$ : Solutions at the previous time step.
- $\Delta t$ : Time step size.

### 3.2.2 2D model: Full Conservation Form

The numerical model in this project is based on the two-dimensional depth-averaged **Shallow Water Equations (SWEs)**<sup>3</sup>, which describe the conservation of mass and momentum in a fluid system. These equations are particularly useful for modeling overland flow, coastal flooding, and other free-surface hydrodynamic phenomena.

The governing equations are expressed in a conservative form as follows:

- **Continuity Equation (Mass Conservation):**

$$\frac{\partial H}{\partial t} + \frac{\partial(Hu_x)}{\partial x} + \frac{\partial(Hu_y)}{\partial y} = 0. \quad (29)$$

This equation ensures the conservation of water depth  $H$  over time by accounting for horizontal fluxes in the  $x$  and  $y$  directions.

- **Momentum Equation in the  $x$ -Direction:**

$$\frac{\partial(Hu_x)}{\partial t} + \frac{\partial}{\partial x} \left( Hu_x^2 + \frac{1}{2}g(H^2 - z^2) \right) + \frac{\partial}{\partial y}(Hu_x u_y) = gh \frac{\partial z}{\partial x} - gn^2 \frac{|u_x|u_x}{H^{1/3}}. \quad (30)$$

This equation describes the momentum changes due to flux variations, pressure gradients, bed slope effects, and frictional resistance in the  $x$ -direction.

- **Momentum Equation in the  $y$ -Direction:**

$$\frac{\partial(Hu_y)}{\partial t} + \frac{\partial}{\partial x}(Hu_x u_y) + \frac{\partial}{\partial y} \left( Hu_y^2 + \frac{1}{2}g(H^2 - z^2) \right) = gh \frac{\partial z}{\partial y} - gn^2 \frac{|u_y|u_y}{H^{1/3}}. \quad (31)$$

Similar to the  $x$ -momentum equation, this governs the forces acting in the  $y$ -direction.

- **Variable Definitions:**

- $H = h + z$  is the total water depth, where  $z$  is the bed elevation and  $h$  is the free surface height.
- $(u_x, u_y)$  are the depth-averaged velocity components in the  $x$  and  $y$  directions.
- $g$  is the gravitational acceleration.
- $n$  is the Manning's roughness coefficient, which accounts for bottom friction.

The equations are written in the *divergence form*. That is, each equation (29), (30), (31) follows the general structure:

$$\frac{\partial U_i}{\partial t} + \nabla \cdot F_i(U) = s_i(U), \quad (32)$$

where  $i = 1, 2$ , or  $3$ , and  $U_i$  represents the  $i$ -th component of the vector  $U^3$  containing the conserved variables:

$$U = \begin{bmatrix} H \\ Hu_x \\ Hu_y \end{bmatrix}. \quad (33)$$

The flux function matrix consists of flux vectors in the  $x$ - and  $y$ -directions, denoted as  $f_x$  and  $f_y$ , respectively:

$$F = [f_x, f_y] = \begin{bmatrix} Hu_x & Hu_y \\ Hu_x^2 + \frac{1}{2}g(H^2 - z^2) & Hu_x u_y \\ Hu_x u_y & Hu_y^2 + \frac{1}{2}g(H^2 - z^2) \end{bmatrix}. \quad (34)$$

The source or sink term vector  $s$  is given by:

$$s = \begin{bmatrix} 0 \\ gh\frac{\partial z}{\partial x} - gn^2\frac{|u_x|u_x}{H^{1/3}} \\ gh\frac{\partial z}{\partial y} - gn^2\frac{|u_y|u_y}{H^{1/3}} \end{bmatrix}. \quad (35)$$

Using these definitions, the equations can be rewritten in the compact form:

$$\frac{\partial U}{\partial t} + \frac{\partial f_x}{\partial x} + \frac{\partial f_y}{\partial y} = s. \quad (36)$$

This formulation provides a physically consistent framework for modeling shallow water flows while incorporating bottom topography effects and frictional dissipation. The model is designed for numerical implementation using the **finite element method (FEM)**, ensuring accurate representation of flow behavior in complex terrains.

**☞ Discontinuous Galerkin Method** <sup>13 24 25 27</sup> For a domain  $\Omega \subset \mathbb{R}^2$ , which is discretized into a set of non-overlapping elements. These elements do not necessarily conform to each other. Let  $X_e$  represent an individual element with its boundary denoted by  $\partial X_e$ .

The numerical solution  $U$  is approximated by  $U_h$ , whose components belong to a space of piecewise smooth functions. These functions are differentiable within each element but will have discontinuities across element boundaries. We denote this function space by  $V_h^4$ .

For any function  $v \in V_h$ , its value on  $\partial X_e$  is defined as  $v^{(\text{in})}$  when evaluated from the interior of an element  $e$ , and as  $v^{(\text{out})}$  when evaluated from the exterior of an element.

**☞ Weak Formulation** The shallow water equations (SWE) are formulated in a discrete weak form by approximating  $U$  with  $U_h$ , multiplying each equation by a test function

---

<sup>3</sup>The scheme for time derivative on  $U$  is defined as:

$$\frac{\partial U}{\partial t} \approx \theta \left( \frac{\frac{3}{2}U^{(n+1)} - 2U^{(n)} + \frac{1}{2}U^{(n-1)}}{\Delta t} \right) + (1 - \theta) \left( \frac{U^{(n+1)} - U^{(n)}}{\Delta t} \right)$$

where for the first two time steps  $\theta = 0$  (first-order implicit Euler scheme) and afterwards  $\theta = 1$  (second-order BDF2 scheme)

<sup>4</sup> $U_h$  belongs to the DG function space  $V_h$ , which is a space of piecewise smooth functions such that  $v|_{X_e} \in H^k(X_e)$  for some  $k \geq 1$ . These functions are locally in Sobolev spaces and hence form local Hilbert spaces, but may have discontinuities across element boundaries.

$v \in V_h$ , integrating over each element, and applying integration by parts to the divergence term:

$$\frac{\partial}{\partial t} \int_{X^e} (U_h)_i v \, dx - \int_{X^e} \nabla v \cdot F_i \, dx + \int_{\partial X^e} (F_i \cdot \mathbf{n}) v \, ds = \int_{X^e} s_i v \, dx, \quad i = 1, 2, 3. \quad (37)$$

Here,  $(U_h)_i$  represents the  $i$ th component of  $U_h$  and  $\mathbf{n}$  is the unit outward normal to the boundary. Since discontinuities are allowed along  $\partial X^e$ , the flux  $F$ , which may be double-valued on  $\partial X^e$ , is replaced in the boundary integral by a single-valued numerical flux to ensure stability and consistency, denoted as  $\hat{F}$ . Substituting this, the discrete weak form becomes:

$$\frac{\partial}{\partial t} \int_{X^e} (U_h)_i v \, dx - \int_{X^e} \nabla v \cdot F_i \, dx + \int_{\partial X^e} (\hat{F}_i \cdot \mathbf{n}) v \, ds = \int_{X^e} s_i v \, dx, \quad i = 1, 2, 3. \quad (38)$$

Here,  $\hat{F}_i$  represents the  $i$ th row of the numerical flux matrix  $\hat{F}$ .

The *Lax-Friedrichs numerical flux*<sup>2</sup> is a common approach in discontinuous Galerkin methods to handle inter-element fluxes. It is defined as:

$$F_{\text{Lax-Numerical}} \rightarrow \int_{\partial X_e} \hat{F} \cdot \mathbf{n} v \, dS = \int_{\partial X_e} (\text{avg}(F(U)) \cdot \mathbf{n}^{(\text{in})} + \lambda \text{jump}(Q)) \text{jump}(v) \, dS \quad (39)$$

where:

- The average operator is given by:

$$\text{avg}(\cdot) = \frac{1}{2} ((\cdot)^{\text{in}} + (\cdot)^{\text{out}}). \quad (40)$$

- The jump operator is given by:

$$\text{jump}(\cdot) = (\cdot)^{\text{in}} - (\cdot)^{\text{out}}. \quad (41)$$

- The Lax-Friedrichs stabilization term  $\lambda$  controls the numerical dissipation to ensure stability.

The value of  $\lambda$  is determined based on the eigenvalues of the Jacobian of the flux tensor, which represent wave speeds in the system. For the shallow water equations, the characteristic speeds include the flow velocity and the gravity wave speed. It is defined as:

$$\lambda = \frac{1}{2} \max \left( \sqrt{(u_x^{\text{in}})^2 + (u_y^{\text{in}})^2} + \sqrt{(gH)^{\text{in}}}, \quad \sqrt{(u_x^{\text{out}})^2 + (u_y^{\text{out}})^2} + \sqrt{(gH)^{\text{out}}} \right). \quad (42)$$

This formula takes the maximum wave speed from both sides of the element boundary, ensuring stability in the numerical scheme.

Boundary conditions modify the weak form by adding terms over the domain boundary  $\partial\Omega$ , which consists of:

- Open boundaries ( $\Gamma_o$ ) where external state  $W_{\text{open}}$  is given.
- Wall boundaries ( $\Gamma_w$ ) where no normal flow is enforced.

The unit normal to the boundary is:  $\mathbf{n} = (n_x, n_y)$ . This is needed to compute fluxes normal to the boundary.

We define:

$$U = (H, Hu_x, Hu_y), \quad (43)$$

$$W_{\text{open}} = (H_{\text{open}}, H_{\text{open}}u_{x,\text{open}}, H_{\text{open}}u_{y,\text{open}}) \quad (44)$$

The velocity vector is:  $u = (u_x, u_y)$ . The normal velocity component:  $u_n = u \cdot \mathbf{n} = u_x n_x + u_y n_y$  which helps in determine the inflow/outflow behavior.

The flux tensor at the open boundary is computed as:

$$\hat{F}_{\text{open}} = \frac{1}{2} (F(U) \cdot \mathbf{n} + F(W_{\text{open}}) \cdot \mathbf{n}) \quad (45)$$

where  $F(U)$  is the flux function for the shallow water system.<sup>5</sup>

To stabilize, a penalty term is added using the jump condition:

$$c_{\text{open}} = \max \left( |u| + \sqrt{gH}, |u| + \sqrt{gH_{\text{open}}} \right) \quad (46)$$

The jump in conserved quantities is:

$$\text{jump}(Q)_{\text{open}} = \begin{bmatrix} H - H_{\text{open}} \\ Hu_x - H_{\text{open}}u_{x,\text{open}} \\ Hu_y - H_{\text{open}}u_{y,\text{open}} \end{bmatrix} \quad (47)$$

Thus, **open boundary condition** in the weak form is modified as:

$$F_{\text{open}} \rightarrow \int_{\Gamma_o} \left( \hat{F}_{\text{open}} \cdot v + \frac{1}{2} c_{\text{open}} \text{jump}(Q)_{\text{open}} \cdot v \right) d\Gamma_o \quad (48)$$

For solid walls, reflective boundary conditions are applied:

The reflected velocity at walls:

$$U_{\text{wall}} = \begin{bmatrix} H \\ u_x n_y^2 - u_x n_x^2 - 2u_y n_x n_y \\ u_y n_x^2 - u_y n_y^2 - 2u_x n_x n_y \end{bmatrix} \quad (49)$$

The flux tensor at the wall boundary:

$$\hat{F}_{\text{wall}} = \frac{1}{2} (F(U) \cdot \mathbf{n} + F(U_{\text{wall}}) \cdot \mathbf{n}) \quad (50)$$

Jump condition for no normal flow:

$$\text{jump}(Q)_{\text{wall}} = \begin{bmatrix} 0 \\ 2Hu_n n_x \\ 2Hu_n n_y \end{bmatrix} \quad (51)$$

---

<sup>5</sup>In the **CG** implementation, the weak form is modified to apply boundary conditions as:  $F = F + (F(W_{\text{open}}) \cdot \mathbf{n}) \cdot v ds(2)$ ;  $F = F + (F(U_{\text{wall}}) \cdot \mathbf{n}) \cdot v ds(1)$  for open( $ds(2)$ ) and wall( $ds(1)$ ) boundaries respectively.

<sup>6</sup>Where  $d\Gamma_o$  refers to open boundary  $ds(2)$

with stabilization coefficient:

$$c_{\text{wall}} = |u| + \sqrt{gH} \quad (52)$$

Thus, the **wall boundary condition** in the weak form is modified as:

$$F_{\text{wall}} \rightarrow \int_{\Gamma_w} \left( \hat{F}_{\text{wall}} \cdot v + \frac{1}{2} c_{\text{wall}} \text{jump}(Q)_{\text{wall}} \cdot v \right) d\Gamma_w \quad (53)$$

After adding these boundary and numerical flux terms, the final weak form is:

$$F = F_{\text{internal}}^8 + F_{\text{open}} + F_{\text{wall}} + F_{\text{Lax-Numerical}} \quad (54)$$

**The  $\alpha$ -Scheme<sup>6</sup> in Finite Element Methods for SWEs to apply Wet-Dry Method** The  $\alpha$ -scheme is a numerical stabilization technique used in Discontinuous Galerkin (DG) finite element methods for solving the shallow water equations (SWEs). It ensures that the water depth  $H$  remains positive, which is crucial for maintaining numerical stability, especially in wetting  $H > 0$  and drying  $H = 0$  scenarios.

- **Prevention of Negative Water Depths:** In numerical simulations of shallow water flows, standard formulations may produce negative water depths due to numerical oscillations, especially in regions with rapidly changing flow. The  $\alpha$ -scheme modifies the water depth variable to ensure non-negativity, preventing unphysical results.
- **Enhanced Numerical Stability:** The standard DG formulation can suffer from stability issues in areas where the water depth approaches zero (dry zones). The  $\alpha$ -scheme acts as a stabilization mechanism by modifying the variables to prevent instability.
- **Comparisons with FVM-Based Methods:** The FVM formulations already include stabilization techniques like the upwind schemes, so incorporating a stabilization mechanism like the  $\alpha$ -scheme in FEM ensures fair comparisons.

The  $\alpha$ -scheme modifies the water depth  $H$ , the bathymetry  $h_b$ , and the flux variables:

$$\tilde{H} = H + f(H), \quad (55)$$

$$\tilde{h}_b = h_b + f(H), \quad (56)$$

$$f(H) = \frac{1}{2} \left( \sqrt{H^2 + \alpha^2} - H \right). \quad (57)$$

where  $\alpha$  is a small positive parameter that ensures  $f(H)$  is always non-negative.

---

<sup>7</sup>Where  $d\Gamma_w$  refers to wall boundary ds(1)

<sup>8</sup> $F_{\text{internal}}$  represents the contribution from the interior elements of the domain in the weak formulation w.r.t the equation (38)

## 4 RESULTS AND DISCUSSION

### 4.1 SWEs in 1D: Test 1 (Comparison of FEM and FVM)

In this study, we simulate the **1D shallow water equations (SWEs)** using the **finite element method (FEM)** in **FEniCSx**, and compare the results with a **finite volume method (FVM)** from the SWE reference paper.

#### 4.1.1 Simulation Setup

Two different test cases were considered with varying Manning's coefficient and wave speed. The following table summarizes simulation parameters used for the two test cases:

Table 1: Simulation parameters for both test cases in 1D

Parameter	Case 1	Case 2
Domain Length ( $L_x$ )	4000.0 m	6500.0 m
Number of Elements ( $nx$ )	150	150
Time Step ( $\Delta t$ )	7.2 s	7.2 s
Total Simulation Time ( $T$ )	9000.0 s	9000.0 s
Constant Wave Speed ( $u_{\text{const}}$ )	0.4 m/s	0.635 m/s
Manning's Coefficient ( $n$ )	$0.01 \text{ s} \cdot \text{m}^{-1/3}$	$0.005 \text{ s} \cdot \text{m}^{-1/3}$

#### 4.1.2 Mesh Resolution and Numerical Stability

During the simulations, it was observed that for **meshes with fewer elements** (e.g., 20, 30, 50, 70 elements), **FEM exhibited oscillations** that were not present in FVM. However, when the **number of elements exceeded 100**, the FEM results showed significantly improved stability and closely matched the FVM results<sup>9</sup>.

This behavior is consistent with the convergence characteristics of finite element formulations for a linearized version of 1D SWEs presented in the SWEMnICS paper<sup>2</sup>. The convergence plots for the  $L^2$  error (between the numerical and analytical solutions) in water depth  $h$  show that the **error decreases at a rate of  $\mathcal{O}(\Delta x^p)$  as the number of elements increases**, where  $p$  is the polynomial order of the approximation and  $\Delta x$  is the element size.

These numerical results validate the convergence of FEM for SWEs in 1D (Our Test 1) and justify the improved performance observed at higher mesh resolutions.

To ensure numerical accuracy and minimize oscillations, a **resolution of 150 elements was used in both test cases**.

---

<sup>9</sup>The Semi-implicit, upwind, and centred schemes of FVM and Roe discussed by De Almeida<sup>1</sup>.

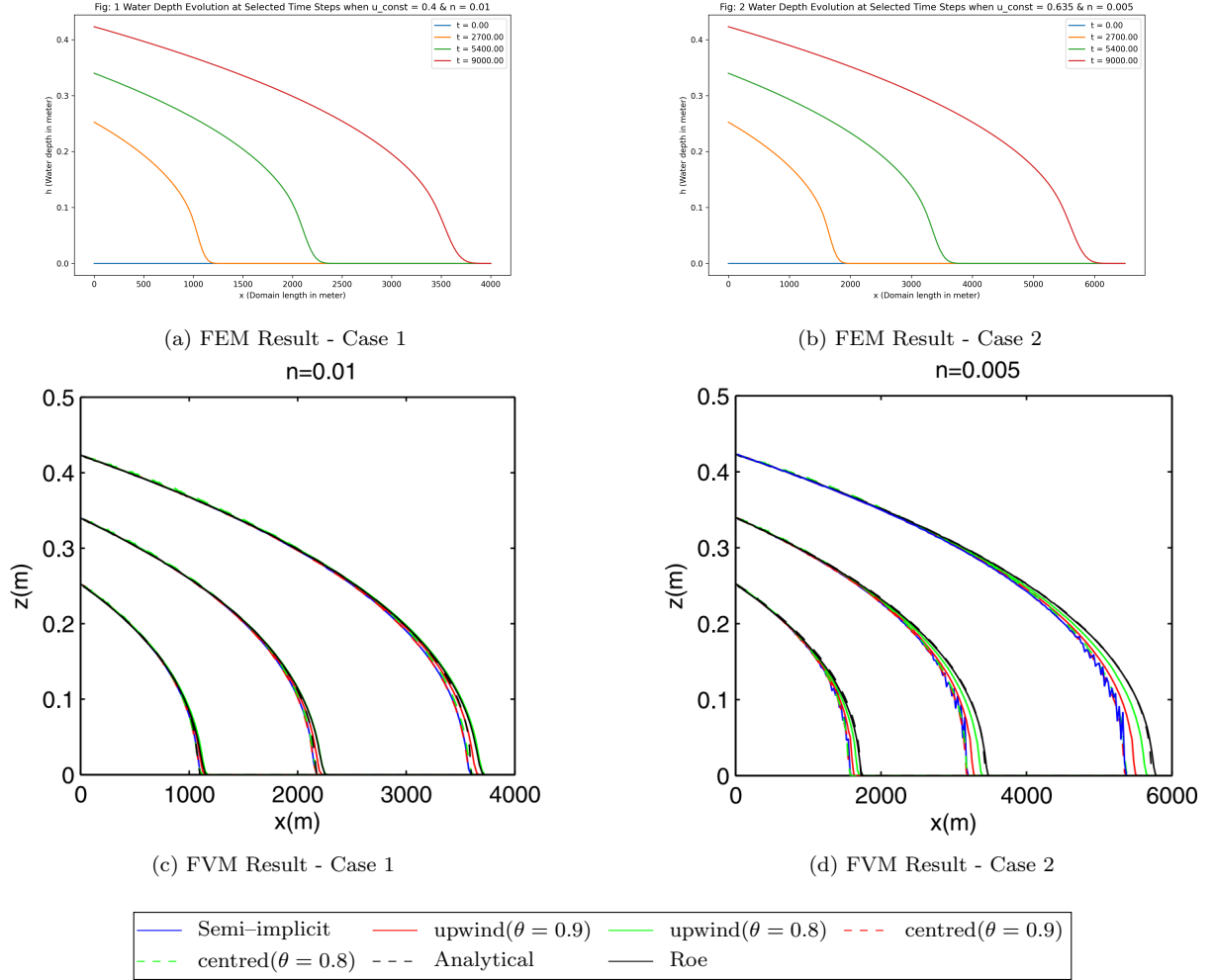


Figure 1: Comparison of FEM (top row) and FVM (bottom row) results for the 1D Shallow Water Equations

The above figures present the **water surface depth** at  $t = 2700s, 5400s$ , and  $9000s$  for two different experimental setups:

Table 2: Summary of Experiments and Corresponding Figures

Experiment	$n$	$u_{\text{const}}$	Figures
Experiment 1	0.01	0.4	Fig. 1a (FEM), Fig. 1c (FVM)
Experiment 2	0.005	0.635	Fig. 1b (FEM), Fig. 1d (FVM)

## Discussion

### Experiment 1:

- Water moves **slower** and does not travel as far in the same time step.
- Represents areas with grass, forests, or rough natural ground (rural area) where **flow encounters significant resistance**.
- The water depth decreases **more steeply** as the flow moves forward.

## Experiment 2:

- Water moves **faster** and reaches farther at the same time steps.
- Represents smoother surfaces like roads, canals (urban area), where water **flows with minimal resistance**.
- The water depth transition is **more gradual**, water spreads out over a longer distance.

### 4.1.3 Effect of Time Step on Mesh Resolution in FEM

During the simulations, it was noticed that the required number of elements in FEM to achieve results comparable to the FVM depends on the chosen time step.

- For **larger time steps**, a **finer mesh** (i.e., more elements) was necessary to suppress numerical oscillations and achieve stable results.
- However, **reducing the time step** allowed for accurate results even with a **coarser mesh** (fewer elements), reducing computational cost while maintaining consistency with FVM.

This highlights the interplay between **spatial and temporal resolution** in FEM for solving the shallow water equations, where an optimal balance must be chosen to ensure numerical stability and efficiency.

## 4.2 SWEs in 2D: Results

### 4.2.1 Test 2: SWEs 2D - Without Bathymetry Experiment with Tidal Wave

This experiment assesses the wetting and drying capabilities of the SWEMnICS framework by employing Kärna's  $\alpha$ -scheme<sup>10</sup> within a CG formulation. The simulation domain consists of a  $13,800 \times 7,200$  m water surface without bathymetry. The mesh resolution is set to:  $nx = 12$ ,  $ny = 6$ . A harmonic tidal forcing (around mean water level) with an amplitude of 2 m and a period of 12 hours is imposed at the open left boundary, while all other boundaries are treated as walls.

The initial condition assumes a flat water surface<sup>10</sup> (Mean water level 0.6 m), and Manning's friction coefficient is set to  $0.02 \text{ s/m}^{1/3}$ . The simulation runs for 7 days with time step size 600s, and water elevations and velocity fields are recorded at three locations:  $x = 9000$  m,  $x = 11,000$  m, and  $x = 13,500$  m ;  $y = 3650$  m. The results, illustrated in Figures 2, 3, and 4, highlight the performance of the  $\alpha$ -scheme in preserving numerical stability while handling wetting and drying processes effectively.

The experiment records temporal evolution of surface elevation and velocity components at three different locations: (9000, 3650) m, (11000, 3650) m, and (13500, 3650) m.

⌚ Station at (9000, 3650) m The plots in Figure 2 show a strong periodic pattern

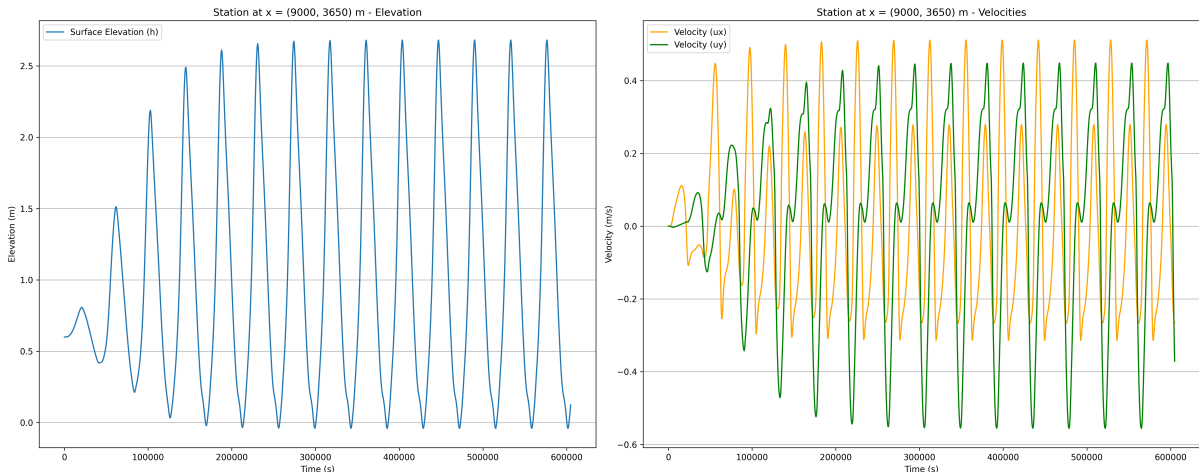


Figure 2: Test 2 (without bathymetry) - Surface elevation and velocity components at station (9000, 3650) m.

in surface elevation around the mean water level 0.6 m, indicating **tidal oscillations or a consistent wave pattern**. The velocity components  $u_x$  and  $u_y$  show oscillatory behavior, aligning with the wave-induced flow dynamics. The **amplitude of oscillations increases after an initial transient phase**.

⌚ Station at (11000, 3650) m Figure 3 shows results at a downstream location. The periodic oscillations remain consistent, but the velocity components  $u_x$  and  $u_y$  show more reduction in peak amplitude than the previous station. This suggests **dissipation or dispersion effects** as the waves propagate further. Additionally, there is an increase in higher-frequency variations in velocity, possibly indicating **nonlinear interactions**.

<sup>10</sup>The bathymetry used in Test 2 is shown in Appendix, Figure 13

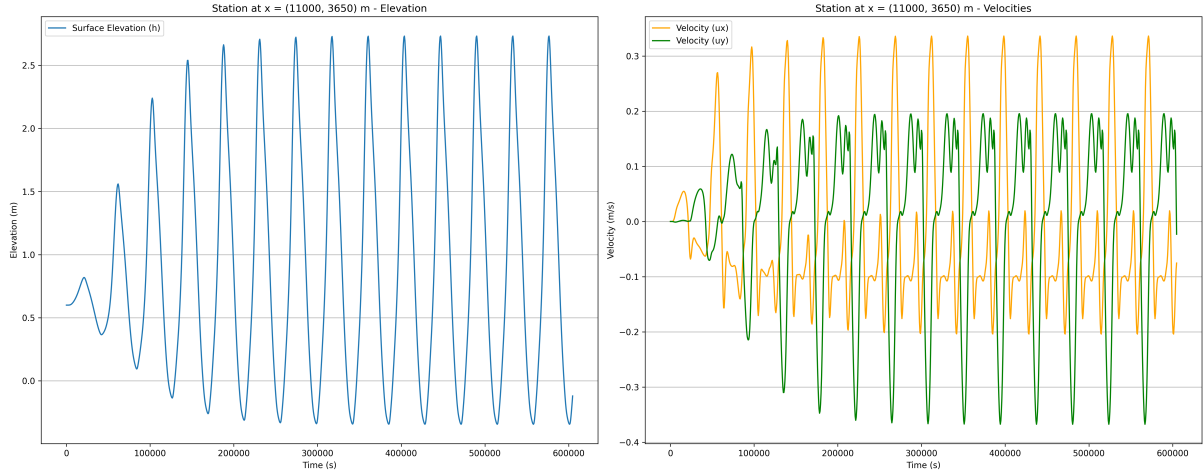


Figure 3: Test 2 (without bathymetry) - Surface elevation and velocity components at station (11000, 3650) m.

### ⌚ Station at (13500, 3650) m

At station (13500, 3650) m, shown in Figure 4, the

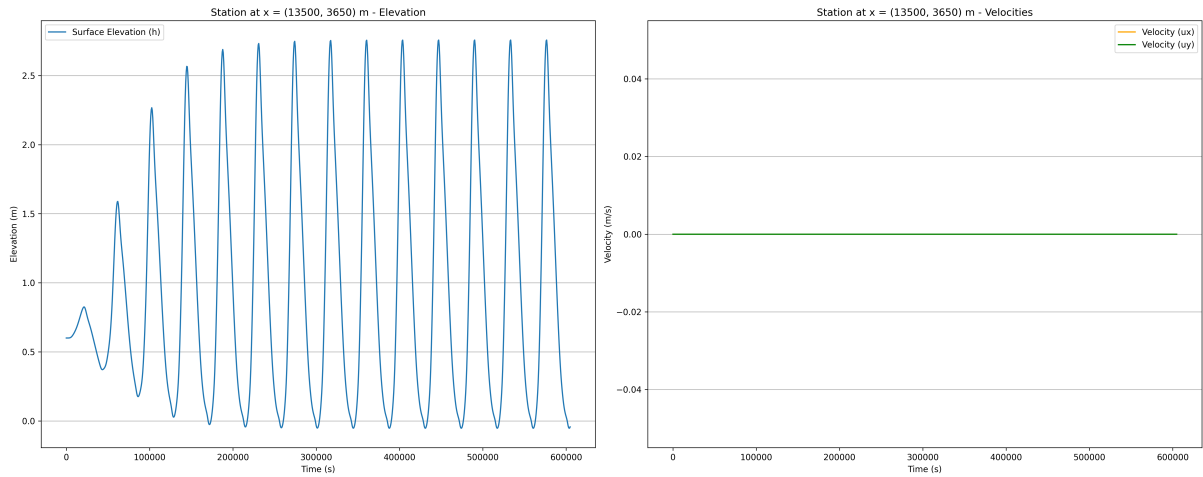


Figure 4: Test 2 (without bathymetry) - Surface elevation and velocity components at station (13500, 3650) m.

surface elevation maintains the periodic pattern, but the velocity components  $u_x$  and  $u_y$  are nearly zero. This is due to **Dirichlet boundary effects for CG elements** as this point is in wall boundary where no flow condition has been applied.

⌚ **Discussion** The results demonstrate a clear propagation of waves with periodic surface elevation changes. However, the velocity fields show **decreasing amplitude with distance**, which may be due to **energy dissipation, numerical diffusion, or boundary conditions**. The zero velocity at the furthest station suggests there is a **Dirichlet boundary effect of zero velocities** at wall boundaries.

Further investigation would include:

- Analyzing the effect of bathymetry on wave propagation.
- Comparing results with CG and DG approach.

## 4.2.2 Test Case Study 1: SWEs on a 2D Sloped Beach (Continuous Galerkin)

This test case evaluates the wetting and drying capability of SWEMniCS using Kärna's  $\alpha$ -scheme with a Continuous Galerkin (CG) approach. The domain consists of a  $13,800 \times 7,200$  m sloping beach. The mesh resolution is set to:  $nx = 12$ ,  $ny = 6$ .

The initial water surface is flat, and a harmonic tide with a 2 m amplitude and 12-hour period is imposed at the open left boundary. All other boundaries are treated as walls. The simulation is run for 7 days with time step size 600s and Manning's friction coefficient set to  $0.02 \text{ s/m}^{1/3}$ .

### ☒ Validation of FEniCS\_Landlab SWE Model Against SWEMniCS Results

This test case presents a validation study of the finite element model implemented in FEniCS\_Landlab for solving the full conservative form of the shallow water equations (SWEs) in 2D. The study is conducted by comparing the results with those obtained using the SWEMniCS model. The accuracy of the model is assessed by computing the  $L_2$  error norm for water surface elevation (height) and velocity components at different stations.

### ☒ Error Analysis

The computed  $L_2$  errors at three stations are presented below:

Table 3:  $L_2$  Errors for Water Surface Elevation and Velocities at Different Stations (CG)

Station	Height ( $L_2$ Error)	X-Velocity ( $L_2$ Error)	Y-Velocity ( $L_2$ Error)
1	$4.562187 \times 10^{-8}$	$1.0796391 \times 10^{-7}$	$1.2659295 \times 10^{-7}$
2	$4.685811 \times 10^{-8}$	$1.2617905 \times 10^{-7}$	$1.8894953 \times 10^{-7}$
3	$2.1687872 \times 10^{-7}$	$1.10390786 \times 10^{-6}$	$2.15778124 \times 10^{-6}$

### ☒ Observations

#### Analysis of WSE from Upstream to Downstream

##### Oscillatory Pattern

- At all three stations (Figures - 5a, 6a & 7a), the WSE follows a periodic oscillatory pattern, indicating the presence of waves or tidal oscillations.
- The oscillations stabilize after an initial transient phase.

##### Amplitude Variation

- Initially (around day 0 to 1), the amplitude of the waves increases as they propagate downstream (Figures - 5a, 6a & 7a).
- By around day 2, the oscillations reach a steady state, maintaining a consistent amplitude (Figures - 5a, 6a & 7a).
- Comparing Station 1 (Figure - 5a) to Station 3 (Figure - 7a), the amplitude remains nearly unchanged, suggesting minimal dissipation of energy.

##### Wave Propagation

- The wave peaks and troughs appear at slightly different times across the stations, indicating a propagation of waves downstream.

- The phase shift is small, meaning the waves travel at a relatively uniform speed along the sloped bathymetry (Figures - 5a, 6a & 7a).

### Analysis of X-Velocity from Upstream to Downstream:

#### Oscillatory Nature of Velocity

- The velocity exhibits a periodic oscillation, indicating a wave-like motion.
- This suggests that the water flow is influenced by tidal flow (Figures - 5b, 6b & 7b).

#### Amplitude Variation Across Stations:

- At Station 1 (Upstream):** The velocity oscillations have higher amplitude compared to downstream stations (Figure - 5b).
- At Station 2 (Midstream):** The oscillations are slightly reduced, indicating a transition in flow characteristics (Figure - 6b).
- At Station 3 (Downstream):** The velocity oscillations show even smaller amplitude, signifying a gradual energy dissipation as the water flows downstream (Figure - 7b).

☞ **Graphical Representation** The following figures illustrate the comparison of water surface elevation and x-velocity at different stations.

#### ☞ Station 1

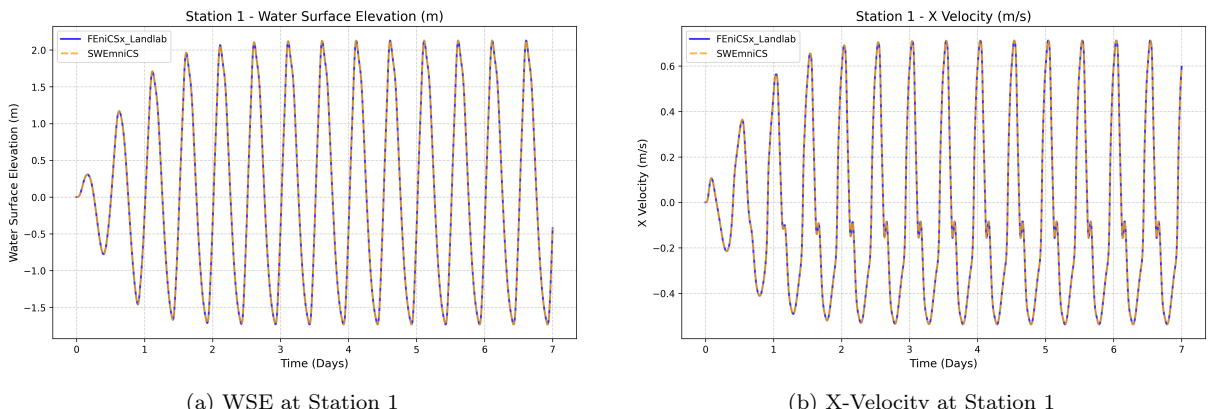


Figure 5: Test Case Study 1 (Sloped Beach - CG): Water Surface Elevation and X-Velocity at Station 1

## ⌚ Station 2

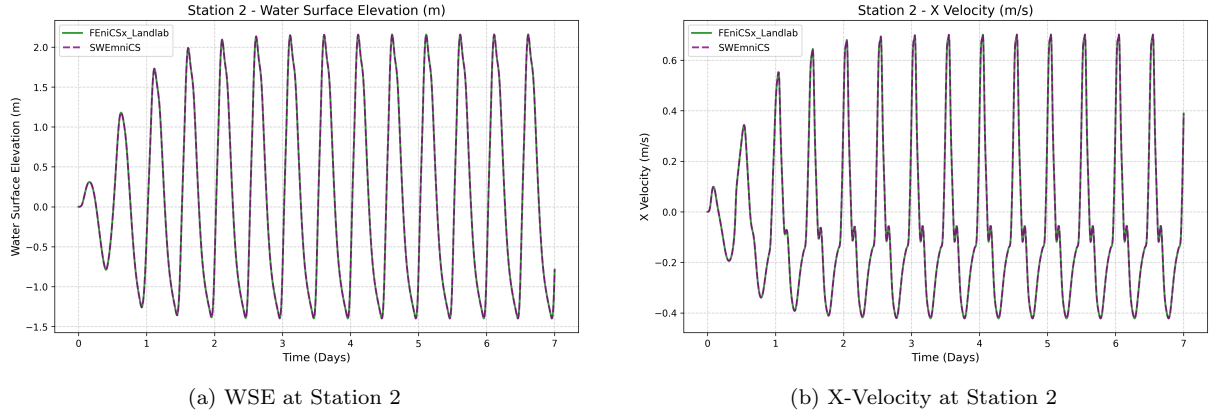


Figure 6: Test Case Study 1 (Sloped Beach - CG): Water Surface Elevation and X-Velocity at Station 2

## ⌚ Station 3

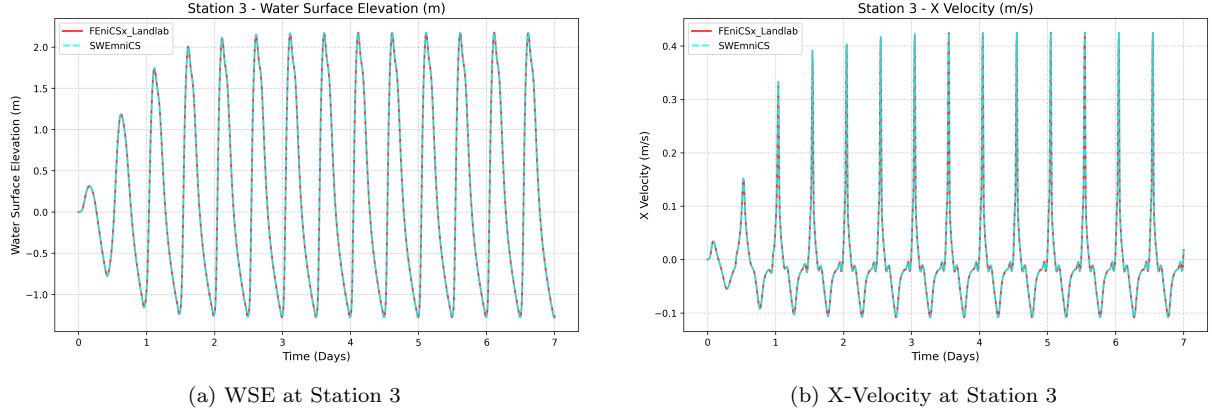


Figure 7: Test Case Study 1 (Sloped Beach - CG): Water Surface Elevation and X-Velocity at Station 3

⌚ **Discussion** The  $L_2$  errors obtained (Table - 3) indicate that the finite element implementation of the shallow water equations in FEniCS\_Landlab closely follows the SWEMniCS results with high accuracy. The errors remain in the order of  $10^{-7}$  for height and in the order of  $10^{-7}$  to  $10^{-6}$  for velocity components.

It is observed that the errors increase at Station 3 (Figure - 7) compared to the other two stations, which could be due to numerical diffusion, boundary effects or sloped bathymetry<sup>11</sup>. The graphical comparison (From Figure - 5 to 7) also demonstrates that the numerical solutions from the two models exhibit similar behavior, validating the implementation.

<sup>11</sup>The bathymetry used in Test Case Study 1 is shown in Appendix, Figure 14.

### 4.2.3 Test Case Study 2: SWEs on a 2D Sloped Beach (Discontinuous Galerkin)

This test case evaluates the wetting and drying capability of SWEMniCS using Kärna's  $\alpha$ -scheme with a Discontinuous Galerkin (DG) approach and the same conditions as above (Test Case Study 1).<sup>12</sup>

#### ☒ Validation of FEniCS\_Landlab SWE Model Against SWEMniCS Results

This presents a validation study of the finite element model implemented in FEniCS\_Landlab for solving the full conservative form of the shallow water equations (SWEs) in 2D with DG elements. The accuracy of the model is assessed by computing the  $L_2$  error norm for water surface elevation (height) and velocity components at different stations.

☒ **Error Analysis** The computed  $L_2$  errors at three stations are presented below:

Table 4:  $L_2$  Errors for Water Surface Elevation and Velocities at Different Stations (DG)

Station	Height ( $L_2$ Error)	X-Velocity ( $L_2$ Error)	Y-Velocity ( $L_2$ Error)
1	0.000138	0.000259	0.000157
2	0.004479	0.052967	0.012717
3	0.010470	0.026956	0.041338

☒ **Graphical Representation**<sup>13</sup> The following figures illustrate the comparison of water surface elevation and x-velocity at different stations.

#### ☒ Station 1

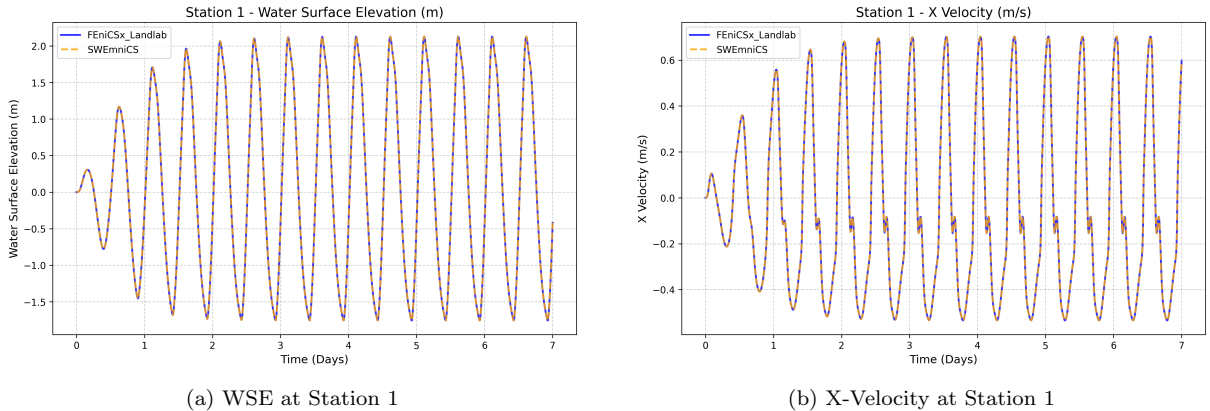


Figure 8: Test Case Study 2 (Sloped Beach - DG): Water Surface Elevation and X-Velocity at Station 1

<sup>12</sup>The bathymetry used in Test Case Study 2 is shown in Appendix, Figure 14.

<sup>13</sup>Same observations for the Test Case Study 2 (Refer to the section 4.2.2 : Observations of Test Case Study 1 with CG elements)

## ⌚ Station 2

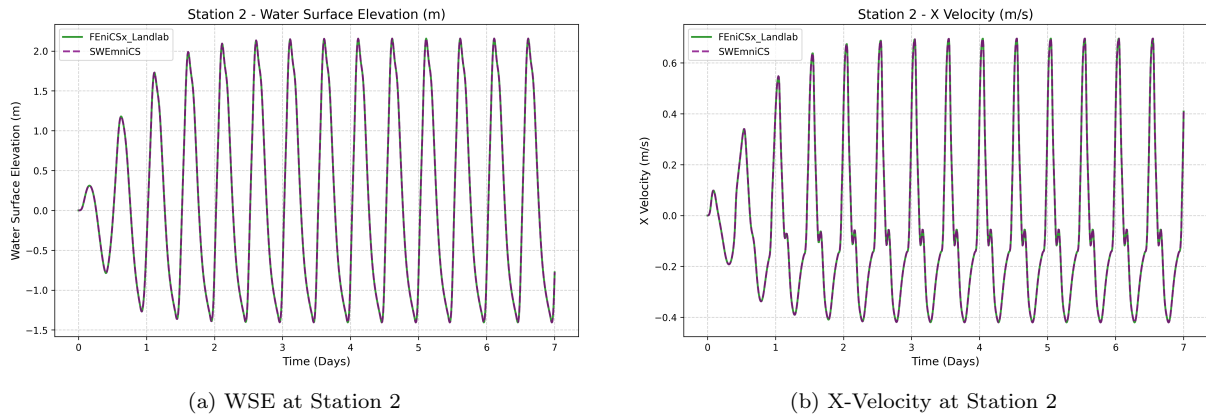


Figure 9: Test Case Study 2 (Sloped Beach - DG): Water Surface Elevation and X-Velocity at Station 2

## ⌚ Station 3

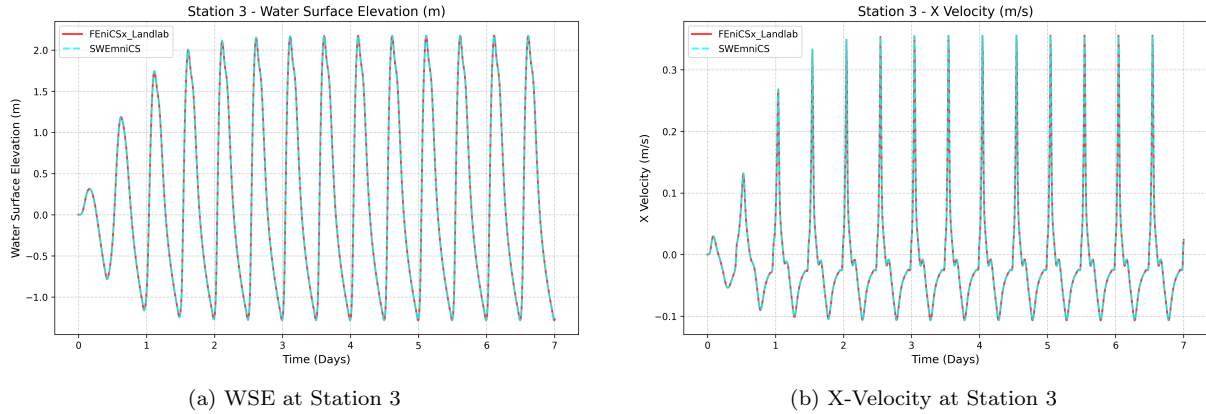


Figure 10: Test Case Study 2 (Sloped Beach - DG): Water Surface Elevation and X-Velocity at Station 3

⌚ **Discussion** The L2 errors indicate the level of difference between the **FEniCSx\_Landlab** and **SWEmniCS** solutions at different monitoring stations. At Station 1 (Figure - 8), the errors are minimal, suggesting strong agreement between the two models.

However, at Station 2 (Figure - 9), the x-velocity error (**0.052967**) is significantly larger than the height and y-velocity errors, indicating a noticeable discrepancy in velocity predictions along the x-direction.

The trend continues at Station 3 (Figure - 10), where the y-velocity error (**0.041338**) is the highest among all components, followed by the height error (**0.010470**), suggesting that differences in water surface elevation are more visible at this location.

These variations could be attributed to numerical diffusion, differences in boundary condition implementations, or mesh resolution differences between the two models. The results highlight that while the models generally align well, have differences locally in velocity and water elevation predictions need further investigation for improved accuracy.

#### 4.2.4 Test 3: SWEs on Real DEM Bathymetry

This experiment evaluates the finite element implementation of the shallow water equations using real-world bathymetry data. The bathymetry is obtained from a DEM file downloaded from **OpenTopography**<sup>14</sup> and processed<sup>14</sup> to generate a suitable computational domain. The experiment follows the same parameters as Test Case Study 1 & 2, with continuous Galerkin (CG) elements.

☞ **Computational Setup** The computational domain<sup>15</sup> is defined using the extracted DEM data. The domain size is determined as:  $L_x = 7739.01$  m,  $L_y = 14811.74$  m as per the dem data. The mesh resolution is set to:  $nx = 6$ ,  $ny = 12$

☞ **Boundary and Simulation Parameters** The boundary conditions are applied:

- **Open boundary:** At  $y = 0$ , a tidal forcing is applied as similar to earlier cases.
- **Wall boundaries:** All other domain boundaries are treated as solid walls with no flow.

The Manning's friction coefficient is set to  $0.02$  s/m<sup>1/3</sup>, and the simulation runs for a total duration of 7 days with time step size 600s.

#### ☞ Analysis of Water Surface Elevation and X-Velocity with CG Elements

This report presents an analysis of water surface elevation and x-velocity at three different stations along a domain with real bathymetry. The simulations were conducted using continuous Galerkin (CG) finite elements for solving the shallow water equations.

The computational domain is analyzed at three stations: **Station 1 - (6450m, 2470m)**, **Station 2 - (6450m, 6180m)**, **Station 3 - (6450m, 11110m)**

#### ☞ Results and Observations

**Water Surface Elevation** Figure 11 shows the water surface elevation at each station. The results indicate periodic oscillations, characteristic of tidal behavior or wave propagation. The amplitude increases slightly from Station 1 (Figure - 11a) to Station 3 (Figure - 11c), suggesting bathymetric influence on wave dynamics.

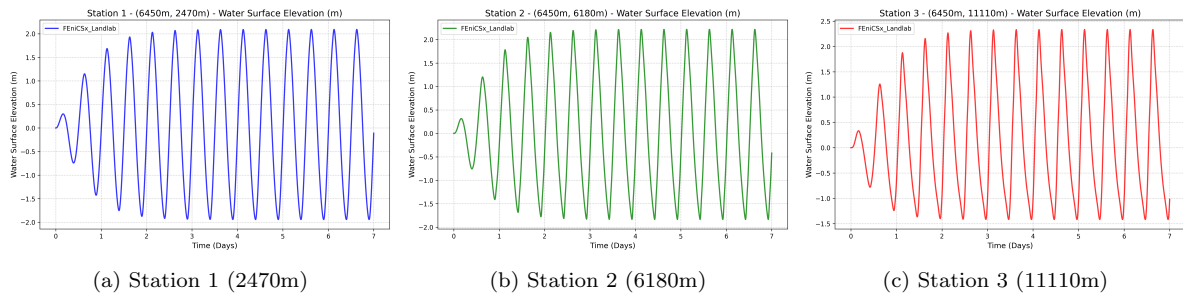


Figure 11: Test 3 (with real bathymetry) - WSE at Different Stations

**X-Velocity** Figure 12 illustrates the x-velocity variations at each station (From Figure

<sup>14</sup>To understand the processing of the DEM Data, refer to Appendix A.3

<sup>15</sup>The bathymetry used in Test 3 is shown in Appendix, Figure 15

12a to 12c). The oscillatory behavior suggests flow reversals, with velocity values fluctuating around zero. Notably, the velocity magnitude is smaller compared to the water surface elevation, indicating a surface-driven flow.

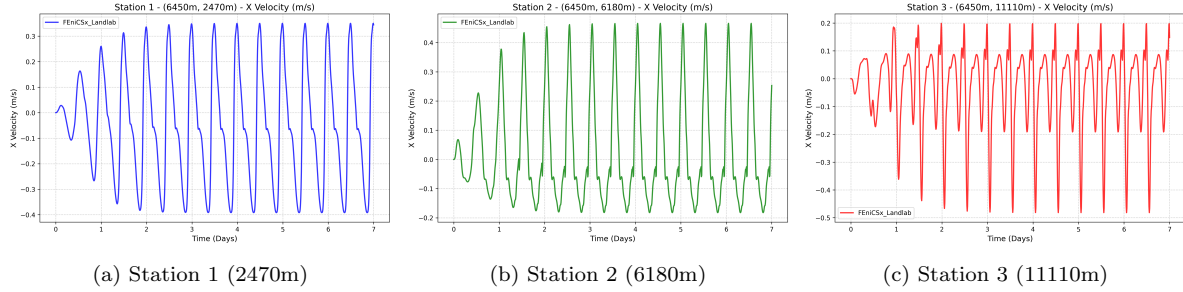


Figure 12: Test 3 (with real bathymetry) - X-Velocity at Different Stations

### Comparison of X Velocity at Different Stations

#### Station 1 (Left, Blue)

- Peaks reach around **0.35 m/s**, and troughs go down to approximately **-0.4 m/s**.
- The waveform is periodic with noticeable sharp peaks.
- The oscillations are well-defined and symmetric.

#### Station 2 (Middle, Green)

- Maximum velocity is slightly higher (**0.45 m/s**), and minimum is around **-0.2 m/s**.
- The oscillations have a nearly similar periodicity to Station 1.
- The waveform appears with sharper peaks compared to Station 1.

#### Station 3 (Right, Red)

- Velocity fluctuates between **-0.5 m/s** to **0.2 m/s**.
- The oscillations appear noisier and exhibit more fluctuations compared to the other stations.
- The peaks are sharper than in Station 1 or 2.

### Discussion

- **Station 1 (smooth, periodic)** → Likely in a relatively stable region with moderate depth (Figure 11a & 12a).
- **Station 2 (higher peak velocities, sharper changes)** → Possibly located in a shallower or constricted region (Figure 11b & 12b).
- **Station 3 (irregular, noisier pattern)** → Might be near a turbulent zone, recirculating flow, or strong bathymetry gradient (Figure 11c & 12c).

The results demonstrate the effectiveness of CG elements in capturing wave behavior over real bathymetry. The increase in water surface elevation amplitude suggests the influence of bathymetric effects. The velocity fluctuations are smaller in magnitude, as expected in shallow water flows. Further investigation into numerical artifacts at Station 2 could be useful for refining the model.

## 5 CONCLUSION AND FUTURE WORK

### 5.1 Summary of Key Findings

This study focused on implementing a FEM-based solver for SWEs using FEniCSx and comparing its performance with existing FVMs, such as the OverlandFlow model in Landlab. Several key findings appeared from the research:

- FEM demonstrated its ability to handle complex topographies effectively, preserving mass conservation residual and stability.
- Numerical experiments showed that the FEM-based solver provided smoother solutions for velocity and water depth while reducing numerical diffusion, a common issue in FVMs.
- The DG formulation demonstrated superior mass conservation compared to the CG approach, with mass conservation residuals on the order of  $10^{-3}$ . This improvement arises because the DG method allows for discontinuities at element interfaces, enabling more accurate flux handling and reducing numerical diffusion. While the CG method enforces continuity across elements, which can introduce artificial smoothing and lead to slight mass loss, especially in sharp gradients or wetting-drying fronts.
- The implementation of **Dirichlet** and **Weakly** boundary conditions influenced the solution accuracy, particularly in capturing flow transitions near boundaries.

### 5.2 Answering Research Questions

Our findings provide insights into the role of mesh resolution, time step size, numerical stabilization, and wetting-drying algorithms in FEM-based hydrodynamic modeling.

- **Effect of Mesh Resolution and Time Step Size:** The accuracy of FEM solutions was found to be highly sensitive to both mesh resolution and time step size. A finer mesh provided improved spatial resolution, reducing numerical diffusion and enhancing solution accuracy, computational costs. The small time steps, while increasing temporal accuracy, also increased computational costs.

For DEM data<sup>16</sup>, increasing the mesh resolution led to Newton solver non-convergence after some time steps (**e.g., 237 steps**). This may be due to the presence of steep gradients or highly irregular terrain features in the bathymetry, which introduce numerical instabilities. Finer meshes can capture more details of the topography but may also create local variations, leading to difficulties in maintaining stability, especially in wetting-drying regions or areas with sharp changes in water depth.

**Role of CFL Condition on Solver Stability -** To better understand the solver instabilities encountered, we estimated the **Courant–Friedrichs–Lowy (CFL) number**, which is a critical parameter influencing stability in numerical simulations of hyperbolic PDEs such as the SWEs. The CFL number is given by:

$$\text{CFL} = \frac{(u + \sqrt{gh}) \cdot \Delta t}{\Delta x} \quad (58)$$

where the notations and the corresponding values are:

---

<sup>16</sup>Refer to section 4.2.4

- $u = 0.333 \text{ m/s}$  is the average of maximum velocity values observed at three stations (as discussed in section 4.2.4),
- $h = 2.23 \text{ m}$  is the average of the maximum water depths at the same stations (as discussed in section 4.2.4),
- $g = 9.81 \text{ m/s}^2$  is the gravitational acceleration,
- $\Delta t = 600 \text{ s}$  is the time step used in the simulation,
- $\Delta x = \frac{L_x}{n_x} = \frac{7739.01}{6} \approx 1289.84 \text{ m}$  is the mesh resolution in the x-direction.

Substituting these values:

$$\text{CFL} = \frac{5.013 \times 600}{1289.84} \approx \frac{3007.8}{1289.84} \approx 2.33$$

This estimated **CFL number of approximately 2.33** exceeds the conventional stability threshold ( $\text{CFL} < 1$ ), which helps to explain the observed instabilities, particularly Newton solver divergence after approximately **237 steps while increasing the mesh resolution**.

This supports the need for a **carefully chosen time step and mesh resolution** that satisfy both the **CFL condition and temporal accuracy**, especially in high-gradient and wetting-drying regions.

- **Numerical Flux Stabilization for High-Gradient Flows:** Numerical stability showed challenges, in high-gradient flows, and dry areas. The inclusion of numerical flux stabilization techniques, such as upwinding and artificial diffusion for DG formulation, significantly improved solution robustness. These techniques reduced unwanted oscillations and maintained stability without compromising accuracy.
- **Effectiveness of the Wetting-Drying Algorithm:** The wetting-drying algorithm played an important role in capturing dynamic water surface variations. The implementation successfully tracked the moving shoreline or WSE, preventing non-physical oscillations in dry regions. Proper parameter tuning in the wetting-drying scheme can make smooth transitions between wet and dry states, which is essential<sup>19</sup> for realistic hydrodynamic simulations.

### 5.3 Practical Applications

The findings from this study have direct implications for hydrological modeling, flood forecasting, and environmental management. Some key practical applications are:

- **Terrain-Based Hydrodynamic Modeling:** The FEM-based solver can be applied to simulations using high-resolution Digital Elevation Model (DEM) data. This allows for accurate representation of real-world topography, improving predictions of overland flow, watershed response, and flood extents in complex terrains.
- **Flood Control:** Modeling stormwater flow in urban environments can help in designing flood control measures, optimizing drainage networks, and assessing the impact of infrastructure development on water flow patterns.
- **River and Coastal Engineering:** FEM-based simulations can assist in designing levees, spillways, and erosion control structures by providing accurate water movement predictions under different hydrodynamic conditions.

## 5.4 Expectations for Future Research

While this research successfully demonstrated the importance of using FEM for solving SWEs, several areas need further investigation:

- **Refinement of Stabilization Techniques:** Explore advanced stabilization methods such as SUPG<sup>2</sup> approach to enhance numerical stability.
- **Hybrid FE Approach(DG-CG) for SWEs:** Implement a combined finite element strategy where the continuity equation is solved using a DG method, while the momentum equations utilize a CG method. This approach uses the DG scheme's strengths in capturing shocks and ensuring local mass conservation while reducing computational cost by taking CG for the momentum equations, hence minimizing the total degrees of freedom.<sup>15</sup>
- **Extending the model to handle unstructured<sup>20</sup> meshes:** Arbitrary domain boundaries allow more accurate representation of complex terrains (e.g, coastlines).
- **Validation with Experimental Data & ML Integration:** Conduct field experiments or using high-resolution remote sensing data to validate simulation results. Use AI and ML techniques to optimize parameter selection and improve accuracy.

In conclusion, this research is a foundation for the application of FEM in overland flow modeling. While challenges remain in terms of computational cost and stability, the potential for improved accuracy and adaptability makes FEM a promising tool for hydrodynamic simulations. Future developments in numerical techniques and computational power will further enhance the applicability of FEM-based SWEs solvers in hydrological studies.

# APPENDIX

## A.1 Numerical Methods

### A.1.1 Finite Element Method for Advection

As an initial case study, the 1D pure advection equation was solved using the finite element method (FEM) in FEniCSx<sup>7</sup>. The numerical solution was validated against an analytical solution following the methodology presented by *Sert*<sup>4</sup>. This study helped in understanding the fundamental behavior of **FEM for hyperbolic PDEs** before moving to the more complex shallow water equations.

### A.1.2 Finite Volume Methods for SWE

Finite volume methods (FVM) have been widely used for solving the shallow water equations (SWE). Various FVM schemes, including **semi-implicit**, **q-upwind**, and **q-centered** methods, were studied based on the work of *Almeida et al.*<sup>1</sup>. These schemes are designed to improve numerical stability and accuracy in flood modeling applications.

### A.1.3 FEM for SWE in 2D

The application of FEM for solving the 2D SWE was explored using the SWEMniCS framework, as described by *Clint Dawson*<sup>2</sup>. This study focused on key aspects such as handling **boundary conditions weakly**, incorporating **numerical flux stabilization**, and implementing a **wetting-drying** algorithm to enhance the robustness of the solution.

## A.2 Additional Figures

### A.2.1 Test 2: Bathymetry Description

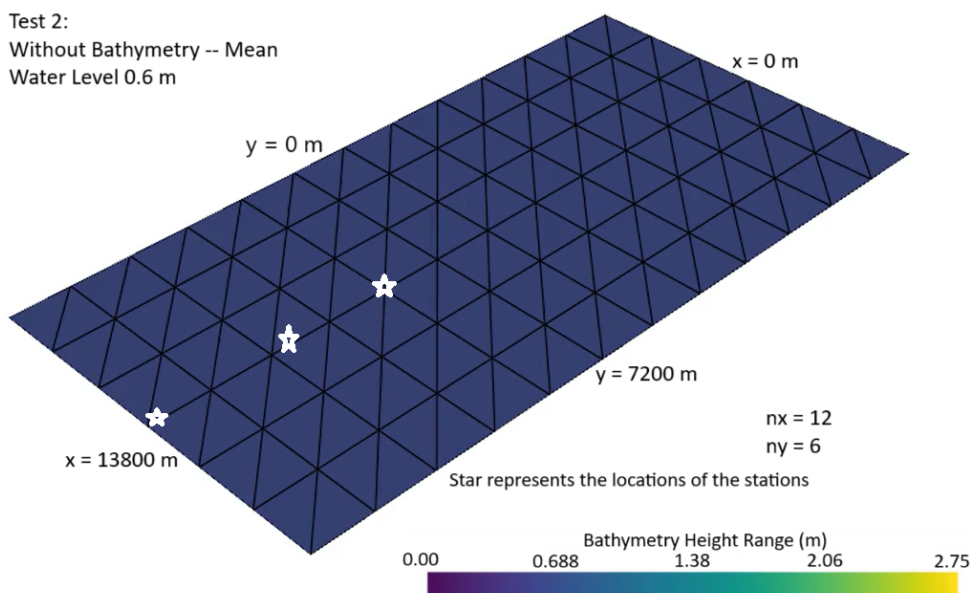


Figure 13: Test 2: Bathymetry

This figure presents the computational domain used in **Test 2: Without Bathymetry**, where the mean water level is set at **0.6 m**. The domain is discretized using a **triangular finite element mesh**, consisting of **12 elements in the x-direction ( $nx = 12$ )** and **6 elements in the y-direction ( $ny = 6$ )**. The black lines indicate the mesh structure.

The **white star markers** represent the locations of the measurement stations where the solution is analyzed.

The **color scale at the bottom** represents the bathymetry height range in meters. However, since this test is conducted **without bathymetry**, the domain is flat with a uniform depth.

The key coordinate values are:

- **x = 0 m** (left boundary) to **x = 13,800 m** (right boundary),
- **y = 0 m** (bottom boundary) to **y = 7,200 m** (top boundary).

This setup is used to analyze how shallow water equations (SWEs) behave in the absence of bathymetry variations, serving as a baseline for comparison with cases that include bathymetric features.

### A.2.2 Test Case Study 1 & 2: Bathymetry Description

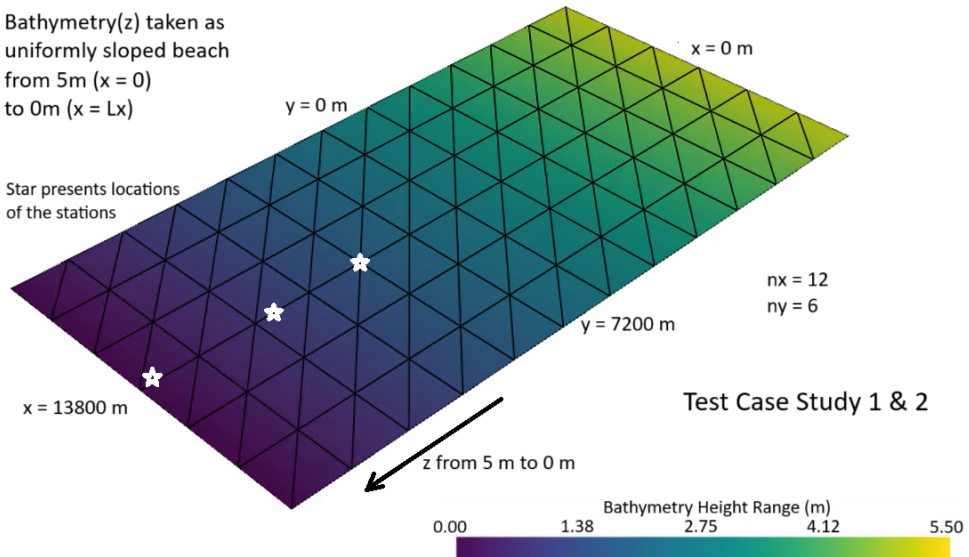


Figure 14: Test Case Study 1 & 2: Bathymetry

This figure presents the computational domain used in **Test Case Study 1 & 2**, where the bathymetry is modeled as a **uniformly sloped beach**. The elevation of the bathymetry (**z**) varies linearly from **5 m** at  $x = 0 \text{ m}$  to **0 m** at  $x = 13800 \text{ m}$  ( $L_x$ ).

The domain is discretized using a **triangular finite element mesh**, with **12 elements in the x-direction ( $nx = 12$ )** and **6 elements in the y-direction ( $ny = 6$ )**. The black lines indicate the mesh structure.

The **white star markers** represent the locations of measurement stations where the solution is analyzed.

The **color scale at the bottom** represents the **bathymetry height range**, which varies from **0.00 m to 5.50 m**. The depth gradually decreases from the left boundary ( $x = 0$ ) towards the right boundary ( $x = 13,800$  m).

The key coordinate values are:

- $x = 0$  m (left boundary) to  $x = 13,800$  m (right boundary),
- $y = 0$  m (bottom boundary) to  $y = 7,200$  m (top boundary).

This setup is designed to analyze shallow water equations (SWEs) over a gradually sloping terrain, representing coastal environments.

#### A.2.3 Test 3: Bathymetry Description

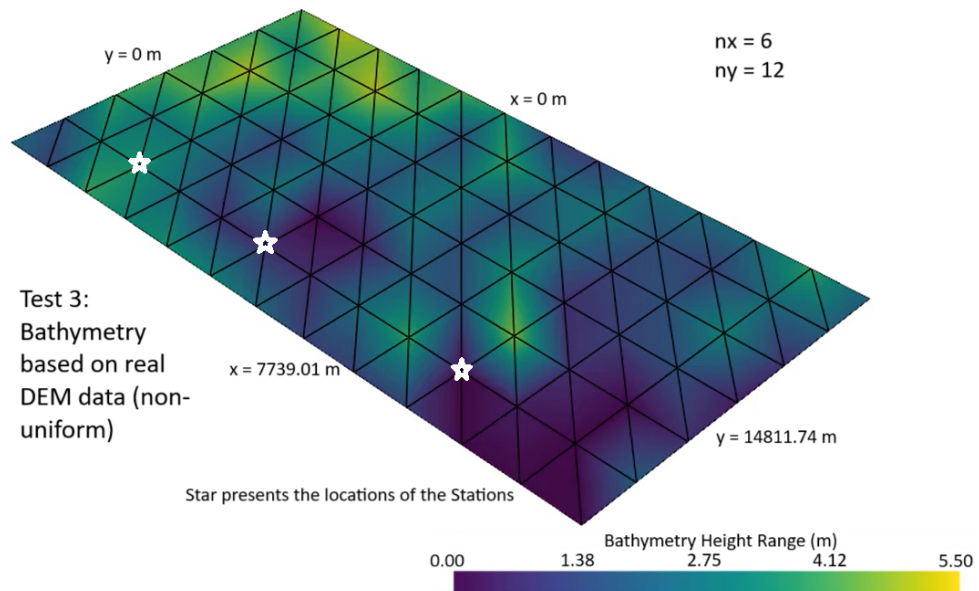


Figure 15: Test 3: Bathymetry

This figure represents the computational domain used in **Test 3**, where the bathymetry is derived from **real DEM (Digital Elevation Model) data**, leading to a **non-uniform topography**.

The domain is discretized using a **triangular finite element mesh** with **6 elements in the x-direction ( $nx = 6$ ) and 12 elements in the y-direction ( $ny = 12$ )**. The black lines illustrate the mesh structure.

The **white star markers** indicate the locations of measurement stations where the numerical solution is analyzed.

The **color scale at the bottom** represents the **bathymetry height range**, which varies from **0.00 m to 5.50 m**. Unlike the previous test cases, the bathymetry in this setup exhibits **spatial variations influenced by the real DEM data**.

The key coordinate values are:

- **x = 0 m** (left boundary) to **x = 7,739.01 m** (right boundary),
- **y = 0 m** (bottom boundary) to **y = 14,811.74 m** (top boundary).

This setup is designed to evaluate the performance of the shallow water equations (SWEs) solver over a **realistic, non-uniform terrain**, allowing for comparisons with natural topographies and real-world hydrodynamic conditions.

### A.3 Processing the DEM Data

To incorporate realistic terrain features into the numerical model, the following steps were performed:

1. **DEM Acquisition:** A digital elevation model (DEM) file in **.tif** format was obtained from **OpenTopography**, representing the bathymetry of a coastal area in **South India (near Chennai)**.
2. **Conversion to CSV:** The DEM raster file was converted into a structured CSV file containing coordinate values (**longitude, latitude**) and **elevation data**.<sup>9</sup>
3. **Transformation to Meters:** Since the DEM data is given in geographic coordinates (**degrees**), it was converted into **meters**. The conversion was based on the **mean latitude** to accurately compute the scaling factors for longitude and latitude.
4. **Normalization of Bathymetry:** The bathymetry values were mapped onto the computational mesh using a nearest-neighbor search with a **KDTree algorithm**. The elevation values were then **normalized** to a range of **[0, 5]** to **ensure numerical stability**

## REFERENCES

- [1] **De Almeida, G. A., Bates, P., Freer, J. E., & Souvignet, M.** (2012). Improving the stability of a simple formulation of the shallow water equations for 2-D flood modeling. *Water Resources Research*, 48(5).
- [2] **Dawson, C., Loveland, M., Pachev, B., Proft, J., & Valseth, E.** (2024). SWEMnics: a software toolbox for modeling coastal ocean circulation, storm surges, inland, and compound flooding. *npj Natural Hazards*, 1(1), 44.
- [3] **Kubatko, E. J., Westerink, J. J., & Dawson, C.** (2006). hp discontinuous Galerkin methods for advection dominated problems in shallow water flow. *Computer Methods in Applied Mechanics and Engineering*, 196(1-3), 437-451
- [4] **Dr. Cüneyt Sert**, ME 582, *Finite Element Analysis in Thermofluids*
- [5] **Valseth, E., & Dawson, C.** (2022). A stable space-time FE method for the shallow water equations. *Computational Geosciences*, 1-18.
- [6] **Kärnä, T., De Brye, B., Gourgue, O., Lambrechts, J., Comblen, R., Legat, V., & Deleersnijder, E.** (2011). A fully implicit wetting–drying method for DG-FEM shallow water models, with an application to the Scheldt Estuary. *Computer Methods in Applied Mechanics and Engineering*, 200(5-8), 509-524.
- [7] **Logg, A., Mardal, K. A., & Wells, G. (Eds.).** (2012). Automated solution of differential equations by the finite element method: *The FEniCS book* (Vol. 84). Springer Science & Business Media.
- [8] **Aricò, C., Sinagra, M., Begnudelli, L., & Tucciarelli, T.** (2011). MAST-2D diffusive model for flood prediction on domains with triangular Delaunay unstructured meshes. *Advances in Water Resources*, 34(11), 1427-1449.
- [9] **Bob Booth**, *Determining a Z-factor for scaling linear elevation units to match geographic coordinate values*
- [10] **Cornel Beffa, Dr. sc. techn.**, 2D-Shallow Water Equations, Basics – Solutions - Applications, *Numerical Hydraulics*
- [11] **Peter Bastian**, *Short Course on Numerical Solution of Hyperbolic Partial Differential Equations*, Interdisziplinäres Zentrum für Wissenschaftliches Rechnen, Universität Heidelberg, Im Neuenheimer Feld 368, 69120 Heidelberg
- [12] **Wang, J. W., & Liu, R. X.** (2005). Combined finite volume–finite element method for shallow water equations. *Computers & fluids*, 34(10), 1199-1222.
- [13] **Aizinger, V., & Dawson, C.** (2002). A discontinuous Galerkin method for two-dimensional flow and transport in shallow water. *Advances in Water Resources*, 25(1), 67-84.
- [14] **Krishnan, S., Crosby, C., Nandigam, V., Phan, M., Cowart, C., Baru, C., & Arrowsmith, R.** (2011, May). OpenTopography: a services oriented architecture for community access to LIDAR topography. In *Proceedings of the 2nd international conference on computing for Geospatial Research & Applications* (pp. 1-8).

- [15] Kirby, R. M., Sherwin, S. J., & Cockburn, B. (2012). To CG or to HDG: a comparative study. *Journal of Scientific Computing*, 51, 183-212.
- [16] Simons, F., Busse, T., Hou, J., Özgen, I., & Hinkelmann, R. (2014). A model for overland flow and associated processes within the Hydroinformatics Modelling System. *Journal of Hydroinformatics*, 16(2), 375-391.
- [17] Liang, D., Lin, B., & Falconer, R. A. (2007). A boundary-fitted numerical model for flood routing with shock-capturing capability. *Journal of hydrology*, 332(3-4), 477-486.
- [18] Hui Pu, J., Shao, S., Huang, Y., & Hussain, K. (2013). Evaluations of SWEs and SPH numerical modelling techniques for dam break flows. *Engineering Applications of Computational Fluid Mechanics*, 7(4), 544-563.
- [19] Song, L., Zhou, J., Guo, J., Zou, Q., & Liu, Y. (2011). A robust well-balanced finite volume model for shallow water flows with wetting and drying over irregular terrain. *Advances in Water Resources*, 34(7), 915-932.
- [20] Costabile, P., & Costanzo, C. (2021). A 2D-SWEs framework for efficient catchment-scale simulations: Hydrodynamic scaling properties of river networks and implications for non-uniform grids generation. *Journal of Hydrology*, 599, 126306.
- [21] Gippel, C. J., & Stewardson, M. J. (1998). Use of wetted perimeter in defining minimum environmental flows. *Regulated Rivers: Research & Management: An International Journal Devoted to River Research and Management*, 14(1), 53-67.
- [22] Hughes, T. J., & Tezduyar, T. (1984). Finite element methods for first-order hyperbolic systems with particular emphasis on the compressible Euler equations. *Computer methods in applied mechanics and engineering*, 45(1-3), 217-284.
- [23] Takase, S., Kashiyama, K., Tanaka, S., & Tezduyar, T. E. (2010). Space-time SUPG formulation of the shallow-water equations. *International Journal for Numerical Methods in Fluids*, 64(10-12), 1379-1394.
- [24] Dawson, C., & Proft, J. (2002). Discontinuous and coupled continuous/discontinuous Galerkin methods for the shallow water equations. *Computer Methods in Applied Mechanics and Engineering*, 191(41-42), 4721-4746.
- [25] Dawson, C., Westerink, J. J., Feyen, J. C., & Pothina, D. (2006). Continuous, discontinuous and coupled discontinuous-continuous Galerkin finite element methods for the shallow water equations. *International journal for numerical methods in fluids*, 52(1), 63-88.
- [26] Navon, I. M. (1988, September). A review of finite-element methods for solving the shallow-water equations. In *Computer Modelling in Ocean Engineering* (Vol. 727). AA Balkema Publishers Rotterdam.
- [27] Wichitnithed, C., Valseth, E., Kubatko, E. J., Kang, Y., Hudson, M., & Dawson, C. (2024). A discontinuous Galerkin finite element model for compound flood simulations. *Computer Methods in Applied Mechanics and Engineering*, 420, 116707.